University of Alberta

Library Release Form

Name of Author: Khanh Quyen Tran

Title of Thesis: Reversing and non-reversing phase transitions in Athabasca bitumen asphaltenes.

Degree: Master of Science

Year this Degree Granted: 2009

_____

University of Alberta

REVERSING AND NON-REVERSING PHASE TRANSITIONS IN ATHABASCA BITUMEN ASPHALTENES

By

Khanh Quyen Tran

A thesis

Submitted to the faculty of graduate studies and research in partial fulfillment of the requirements for the degree of Master of Science in Chemical Engineering

Department of Chemical and Material Engineering

Edmonton, Alberta

Spring 2009

University of Alberta

Faculty of Graduate Studies and Research

The undersigned certify that they have read, and recommend to the Faculty of Graduate Studies and Research for acceptance, a thesis entitled Reversing and Non-reversing Phase Transitions in Athabasca Bitumen Asphaltenes by Khanh Quyen Tran in partial fulfillment of the requirements for the degree of Master of Science.

_____

Prof. John M. Shaw

_____

Prof. Phillip Y. K. Choi

_____

Prof. Carlos F. Lange

Date: _____

Abstract

The phase behaviour of Athabasca bitumen asphaltenes separated from their native hydrocarbon resource using normal alkanes was studied using differential scanning calorimetry (DSC) and temperature modulated differential scanning calorimetry (TMDSC) measurements in the temperature range 300 K to 520 K. For pentane through dodecane Athabasca bitumen asphaltenes, there is a broad reversible endothermic transition, from solid to liquid, overlapping an irreversible exothermic transition in the temperature range 330 K and 520 K. Thus, in general, asphaltene thermal properties and hence phase behaviour differ depending on their thermal history above 330 K.

The starting temperature of the non-reversing transition was found to be 380 ± 8 K. The end temperatures increased linearly from heptane to dodecane asphaltenes; pentane and hexane asphaltenes have the same end temperature, which is higher than for the other asphaltenes.

Acknowledgments

This work would not have been possible without the support and encouragement of my supervisor and mentor, Dr. John M. Shaw. His enthusiasm to teach, combined with a unique sense of humour, was a constant source inspiration throughout my research. I would also like to take this opportunity to thank Dr. Yadollah Maham for his guidance about calorimetry and his support and encouragement during my time at University of Alberta, Dr. Michal Fulem for his advice about this project, Ms. Mildred Becerra for her help with preparing asphaltenes samples, and Dr. Mike Xia for his assistance with TMDSC at National Institute for Nanotechnology (NINT).

I also acknowledge the scholarship program at the University of Alberta and research funds from the sponsors of the NSERC Industrial Research Chair in Petroleum Thermodynamics (Alberta Energy Research Institute, ConocoPhillips, Halliburton Energy Services Ltd., Imperial Oil Resources, KBR, NEXEN, Shell Canada Ltd., Total E&P Canada, and NSERC).

I also extend my gratitude towards Mr. Nouman Noor, whose encouragement, support and dedication was a constant source of motivation and inspiration. I cannot end without thanking my parents, my father Sanh Vinh Tran and my mother Nga Thi Duong, on whose constant encouragement and love I have relied throughout my time at the University of Alberta. It is to them I dedicate this work.

Table of Contents

List of Figures

List of Tables

CHAPTER 1 – INTRODUCTION

Crude oils are complex mixtures of primarily hydrocarbon compounds. Often these components are divided into saturated and unsaturated hydrocarbons, aliphatics, aromatics, resins, and asphaltenes. There are two main types of crude oils: light oils and heavy oils. Light oils are highly fluid, often clear, spread rapidly on solid or water surfaces, have a strong odour, a high evaporation rate, and are usually flammable. Unlike light oils, heavy oils have much higher molecular weight; they are very viscous and do not flow easily. The common characteristic properties of heavy oils are high specific gravity and viscosity, low hydrogen to carbon ratios (H/C), and high contents of asphaltenes, heavy metal, sulphur and nitrogen.

The current trend in the petroleum refining industry is to make greater use of heavy crude oils. These feed stocks are more difficult to process due to higher contents of heteroatoms, asphaltenes, metals and larger quantities of non-distillable hydrocarbons when compared with light crude oils[1]. Asphaltenes are a problem due to their tendency to associate and precipitate during both oil production and refining. They reduce oil flow or even cause blockages during production and cause severe drawbacks during the processing of heavy ends such as the tendency to form coke deposits in reactors, and to deactivate or poison catalysts.[2]

Asphaltenes are defined in the literature according to their solubility in non-polar solvents and not by their chemical structure. They are defined as a fraction that precipitates upon the addition of an *n*-alkane, to form micron sized aggregates, but which do not form such aggregates when mixed with aromatic solvents such as toluene[3]. Changes in pressure, temperature, and/or composition can also cause asphaltene precipitation. For example, when the pressure is lower around and within well bores than in a reservoir, asphaltenes can precipitate and production can be reduced significantly. In addition, when condensate is used as a diluent with heavy oils to facilitate separation from water or mineral matter or to reduce viscosity, asphaltene deposition can also occur in surface facilities and pipelines[3].

The characterization of asphaltenes has been the subject of much research and debate, and there is a general agreement that asphaltenes contain condensed aromatic molecular sub units in addition to naphthenic, alkyl, cycloalkyl, heteroatom constituents such as sulphur, nitrogen, and oxygen, and the major portion of nickel and vanadium[2, 4-6]. Since asphaltenes are a complex mixture defined operationally, rather than a pure compound, they are difficult to characterize. The studies of Calemma et al.[2, 5] and Pacheco-Sanchez et al.[7] indicated that asphaltene molecules have a wide range of molecular weights and structures depending on their origin, as illustrated in Figure 1-1 from Takanohashi et al.[8]. Calemma et al.[2] studied the characteristics of seven different origin asphaltenes (Gela, Belayim, Safaniya, Arabian Light, Brent, Gaggiano, and Villafortuna) to provide a better understanding of their analogies and peculiarities. Their study showed several significant trends in molecular structure with increasing carbon content, which can be summarized as follows: as aromaticity increases, the average length of alkyl side chains decreases, the heteroatom content lowers, the average molecular weights become smaller; and the average aromatic core size increases[2]. Also, Leon et al.[9] showed that asphaltenes from unstable crude oils have a lower hydrogen content, higher aromaticity, and higher degree of aromatic condensation than those from stable crudes. There might be a link to the geology and maturity of the reservoir. Marine (ocean bottom-deposited), lacustrine (lake-bottom-deposited), and terrestrial are three type of oil shales that are classified by Hutton[10] and this classification is useful in estimating the yield and composition of the extracted oil.

Pericondensed and archipelago structures are the two fundamental structure models that are used to categorize asphaltene structure in the current literature[6]. The pericondensed structure was used by Takanohashi et al.[8] to construct molecular models for three different asphaltenes, Figure 1-1. Sheremata et al.[6] generated a quantitative molecular representation of Athabasca asphaltenes using an archipelago structure, Figure 1-2, that was consistent with data from elemental analysis, H and ^{13}C NMR spectroscopy, and vapor-pressure osmometry. Sheremata et al.[6] also showed that asphaltenes from a single source must be characterized using more than one molecule having different structures and molecular weights. As a result of the uncertainty regarding even their average

structure, it is difficult to predict asphaltene phase behaviour, and physical properties other than their heat capacity in the solid state [11-14]. Detailed evaluation and understanding of asphaltene phase behaviour, in particular, would be a valuable aid to practitioners who develop, design, or operate heavy oil or bitumen production, transport and refining processes.

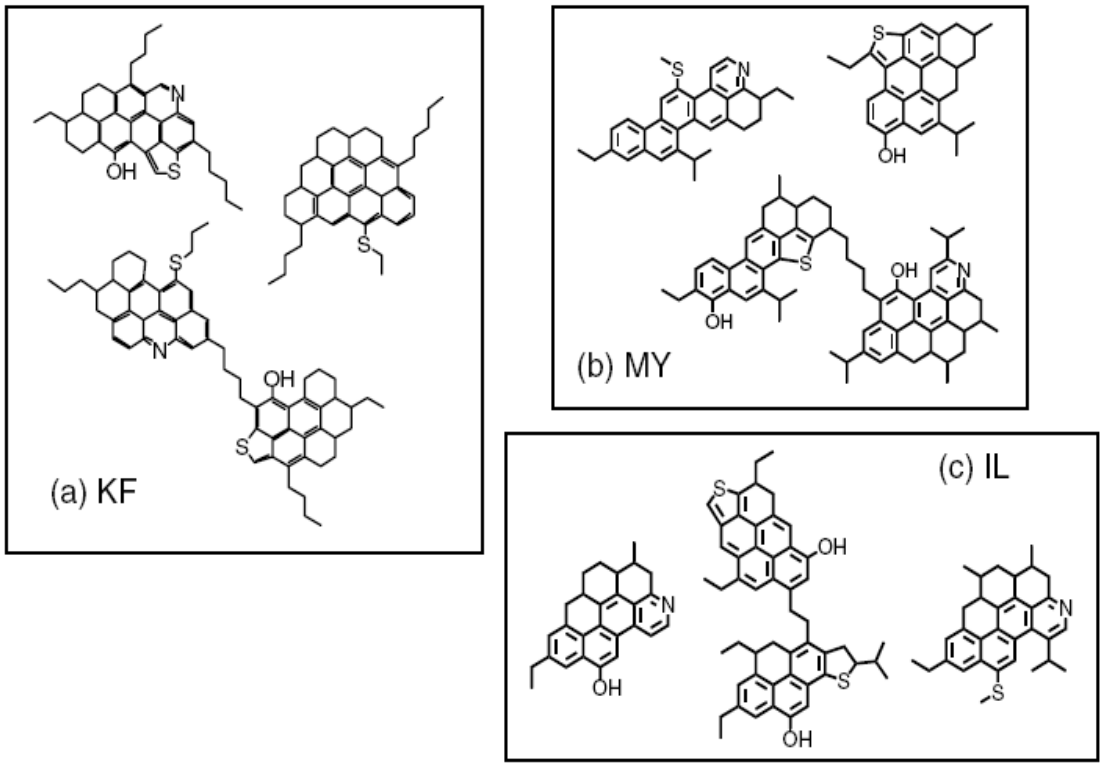

Figure 1-1: Pericondensed structures for a) Khafji, b) Maya, and c) Iranian-Light asphaltenes[8]

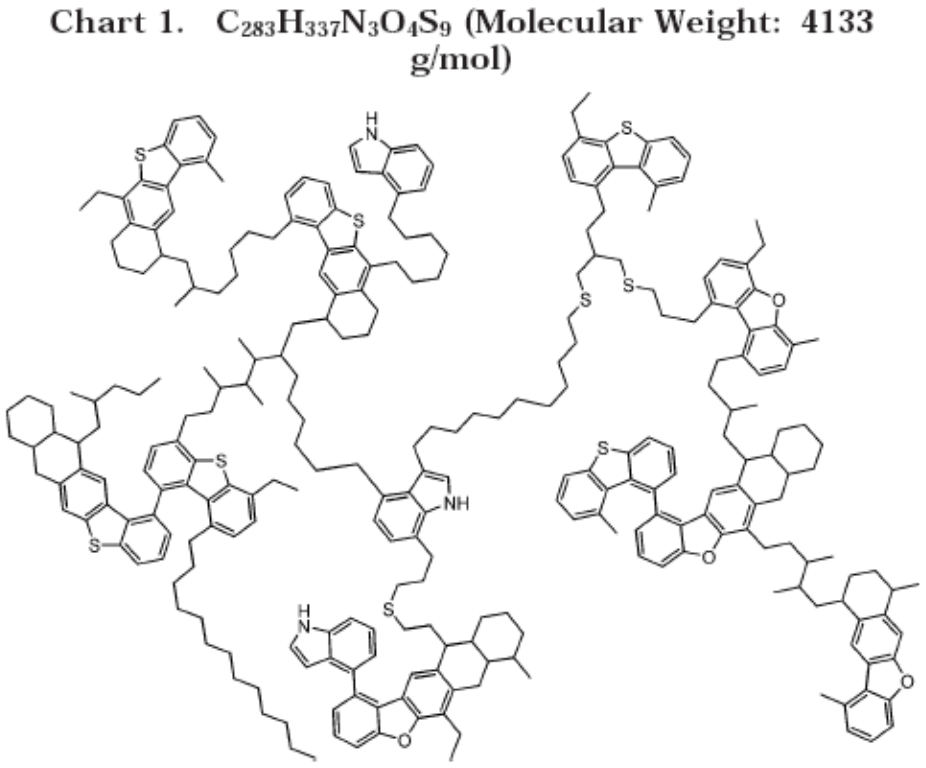

Figure 1-2: Archipelago structure for Athabasca asphaltene with molecular weight of 4133 g/mol[6]

This thesis addresses phase transitions occurring in asphaltenes and focuses on two specific questions:

1. Are phase transitions occurring in asphaltenes reversible?
2. Are phase transitions occurring in asphaltenes affected significantly by the details of their definition?

Solution behaviour and differences in solution behaviour with asphaltene definition are not a focus of this work. In the balance of the thesis, the relevant literature concerning the definition and phase behavior of asphaltenes is reviewed (chapter 2). Experimental methodologies used are described (chapter 3). Detailed descriptions of experiment procedures for asphaltene preparation, phase behaviour evaluation and data analysis are also presented. Results are reported and discussed (chapter 4). Key conclusions and recommendations for future study are then presented (chapter 5).

CHAPTER 2 – LITERATURE REVIEW

2.1 – Definition of Asphaltenes

Asphaltenes are the heaviest constituents of crude oil; believed to be present as colloidal particles which give the oil a black-brown colour[15]. In general, asphaltenes are characterized by fused ring aromaticity, small aliphatic side chains, and polar heteroatom containing functional groups. Asphaltenes are operationally defined as a non-volatile and polar fraction of the crude oil that is insoluble in *n*-alkanes yet is soluble in aromatic solvents such as toluene[4, 14]. Typically, asphaltenes aggregates can be filtered from dilute mixtures including *n*-alkanes using filters with nominal pore sizes in the micron range; however, they will pass through a filter with the same nominal pore size when dispersed in aromatic solvents[14].

The precipitation of asphaltene aggregates can cause severe problems such as reservoir plugging and wettability reversal resulting in a critical need of quantitative tools and thermodynamic data to predict asphaltene solubility and aggregation as a function of crude composition and reservoir temperature and pressure. The solubility class definition of asphaltene generates a broad distribution of molecular structures that can vary greatly in size and polarity from one crude to another[16]. Speight et al.[17] studied the factors influencing the separation of asphaltenes from heavy petroleum feedstock. Several methods have been applied as a means of asphaltene separation prior to characterization studies. Elements of separation, such as ratio of aromatics to solvents and resin to asphaltenes in crude together with precipitant type and aging time are important variables which greatly influence the characterization of asphaltenes[17]. Speight compared the various parameters that can be applied (as well as the necessity for these parameters) to the separation of asphaltenes to bring attention to the general problems of asphaltenes separation.

Speight et al.[17] pointed out that substituting separating medium *n*-heptane (IP 143/57, ASTM D3279-76, IP 143/77, and ASTM May1977) for n-pentane (ASTM D893-69, Syncrude Analytical, ASTM D2006-70, and ASTM D2007-75) can yield asphaltenes that differ in aromaticity (H/C atomic ratio) and molecular weight. *N*-pentane is preferred if the deasphalted oil is to be further subdivided by adsorption chromatography with minimal adsorbent hold-up; however, *n*-heptane separation is preferred if a more stable asphaltene is desired[17]. Furthermore, other parameters such as feedstock/hydrocarbon ratio, contact time, and temperature also affected the amount and quality of asphaltene separated. Again, these parameters also depend on the solvent used[17].

Furthermore, Yarranton and Masliyah[18] successfully modeled asphaltene precipitation in solvents by treating asphaltenes as a mixture of components of different density and molar mass. They found that a small variation in asphaltene solubility parameter with molar mass can significantly affect the prediction compared with a first-order solubility parameter[18].

2.2 – Asphaltenes and Phase Transitions

2.2.1 – Phase Behaviour Observations with Neat Asphaltenes

Asphaltenes are molecules with high solubility parameters and moderately high molecular weight[19-23] that associate strongly with one another. This latter property is built into their definition – by precipitation. The phase behaviour of asphaltenes has mainly been studied in terms of their solution behaviour in mixtures[24-28] or in native oils (Maya crude phase diagram just published by our group)[29] rather than on their own. Some works have addressed the phase behaviour of asphaltenes in solution. For example, Evdokimov et al.[26, 27] studied the behaviour for solutions of asphaltenes and heavy crudes by dynamic viscosity, NMR, and optical absorption. Their study showed that asphaltenes may undergo a liquid-liquid phase separation into glassy noncoalescenting "droplets". Sirota et al.[25, 28] studied glass transitions of asphaltenes by relating the viscosity of bitumen + asphaltene mixtures. The asphaltenes + liquid mixtures literature is not a focus for this work. The focus of this work is to understand

the driving forces and the strengths of the driving forces linked to their association[30-32]. However, the asphaltene "solution" literature provides some clues with respect to expected behaviours in general and whether transitions observed in solution, such as asphaltene precipitation, are reversible. By analogy, these may apply to neat asphaltenes as well. Precipitation, for example, is viewed to be only partially reversible[33, 34].

The thermal behaviour of neat asphaltenes has been studied by many researchers. Zhang et al.[35] studied glass transition temperatures of asphaltenes using differential scanning calorimetry. They reported that the glass transition temperature for four different asphaltenes from different vacuum residues (Iranian Light, Khafji, Kuwait, and Maya) was around 393 K. It was found that asphaltenes started to soften at around 423 K and attained a completely liquid state at temperatures between 493 K and 513 K. However, Gray et al.[36] reported melting temperatures of four different asphaltenes (Arab Light and Heavy, Athabasca, Gudao, and Maya) that were in the range 497 K – 567 K with standard deviations 16 K – 19 K. The study by Gray et al.[36] was conducted by rapidly heating thin films of asphaltenes. Within the standard deviation, the temperature range found by Gray et al.[36] and Zhang et al.[35] agreed at lower limit; however, the upper temperature limit from Gray et al.[36] was higher from what found by Zhang et al.[35]. The difference could be due to the different origin of the crude oils and the speeds of the tests relative to phase transition kinetics.

Maham et al.[37] studied the phase behaviour of Athabasca vacuum bottoms (ABVB) asphaltenes using SAXS, X-ray transmission, and differential scanning calorimetry. Their study indicated that asphaltenes exhibit a heat capacity consistent with that of an ordered solid at temperatures below 260 K. They also found that asphaltenes and asphaltenes in *n*-alkanes solvents or native oils can exhibit polymorphism, and that asphaltenes may also comprise two phases over a broad range of conditions. The study for heat capacity of ordered solids at low temperatures was computed from molecular structure on the basis of the vibration frequency spectrum for the molecular constituents and such calculations were performed for polymers[37]. Also, their study showed ABVB asphaltenes exhibit phase transition at lower temperature on cooling than on heating in a

systematic manner. A broad endothermic transition arises at 260 K; an exothermic transition that drives the apparent heat capacity of asphaltenes below the heat capacity of rigid organic crystals begins to dominate around 350 K. The endothermic and exothermic processes observed were shown to be reversible. Maham et al.[37] suggested that one fraction of the asphaltenes undergoes melting or a glass transition (endotherm) while another fraction dissolves into it (exotherm) at higher temperature. This work on phase transitions in asphaltenes and heat capacity of solids including asphaltenes was updated with a recent series of publications[29], and solids heat capacity respectively [11, 12] which included pentane asphaltenes. The heat capacity reports, the rheological measurements and calorimetric measurements all reinforce the contention that asphaltenes are solids at low temperatures and that they undergo a broad endothermic transition to liquid at higher temperatures. The more recent and more precise calorimetric measurements[29] indicate the presence of a slowly reversing, if not reversible transition at high temperature ~ 573 K for Maya pentane asphaltenes. Zhang et al.[35] also reported that a glass transition in Iranian Light, Khafji, Kuwait, and Maya asphaltenes was not reversible on the time scale of their measurements.

2.2.2 – Objectives

Phase transitions of asphaltenes are known phenomena and have been a focus of many studies in the past. However, little research has been conducted in order to understand the reversibility of asphaltene phase transitions and the variation of transition conditions with asphaltene definition. Studies, such as those conducted by Evdokimov et al.[26, 27] and Sirota et al.[25, 28] indicate the possibility of a reversible phase transition for asphaltene samples in solutions while Zhang et al.[35], Gray et al.[36], Maham et al.[37], and Fulem et al.[29] indicate the reversibility of asphaltenes without any solvents. However, high quality experimental data are required to assess the issue more thoroughly. This research compares experimental phase transition data obtained via Differential Scanning Calorimetry (DSC) and Temperature Modulated Differential Scanning Calorimetry (TMDSC) to those in the literature in order to better understand the reversibility of

asphaltene phase behaviour and the impact of asphaltene definition on the conditions where transitions occur.

CHAPTER 3 – EXPERIMENTAL

3.1 – Methodology

Both conventional Differential Scanning Calorimetry (DSC) and Temperature Modulated Differential Scanning Calorimetry (TMDSC) are employed in this study. They are both required because of the contrasting strengths of these two techniques and careful calibration is required for both methods to yield quantitative data.

3.1.1 – Conventional DSC

3.1.1.1 – Technique Overview

Differential Scanning Calorimetry (DSC) is a well establish thermal analysis technique which is used on a large scale in different areas of research, development, and quality inspection and testing. DSC means the measurement of the change of the difference in the heat flow rate to the sample and to a reference sample while they are subjected to a controlled temperature program[38]. Over a large temperature range, thermal effects can be quickly identified; the heat capacity, heat of transition, kinetic data, purity, and glass transition of a substance can be determined with the relevant temperature and the characteristic caloric values obtained by DSC. Furthermore, DSC curves can be used to identify substances, to set up phase diagrams and to determine degree of crystallinity[38].

There are two basic types of DSC in common use: the heat flux DSC and the power compensation DSC. The heat flux DSC is used in heat-exchanging calorimeters. The heat measured takes place via a heat conduction path with given thermal resistance. The temperature difference is the primary measurement signal; it determines the intensity of the exchange and the resulting heat flow rate is proportional to it. The power compensation DSC is normally used in heat-compensating calorimeters; the heat measured is compensated with electric energy by increasing or decreasing an adjustable

Joule's heat. In power compensation DSC, the temperatures of the sample and reference are controlled independently using separate identical furnaces[39].

3.1.1.2 – Theory:

Since the DSC used in this study was heat flux DSC, only the principle of a heat flux DSC is discussed in this section.

The steady-state and non-steady-state processes were considered in the heat flux DSC. In the steady-state process, it was assumed that the heat flow rate is constant, only one thermal resistance is taken into account with no interaction between sample and reference sample, only the heat capacities of the sample and reference sample are taken into account, and no heat exchange is lost to the surrounding[40].

A combination of the Biot-Fourier equation of the steady-state conduction of heat and the formation in absolute values can be written as follows:

$$\frac{\overline{\Phi}}{A} = -\lambda \cdot grad \quad T \qquad \text{or} \qquad \frac{|\overline{\Phi}|}{A} = -\lambda \cdot |\, grad \quad T\,| \tag{3.1}$$

With Φ, A, λ, and T are heat flow rate, cross section area, thermal conductivity, and temperature, respectively. The amount of heat flux Φ/A is proportional to the gradient of the temperature; the thermal conductivity, λ, is the proportionality factor.

Equation (3.1) is reduced as follows for the sample (S) and reference (R):

$$\frac{\Phi_{FS}}{A} = -\lambda \cdot \frac{(T_F - T_S)}{\Delta l} \qquad \text{and} \qquad \frac{\Phi_{FR}}{A} = -\lambda \cdot \frac{(T_F - T_R)}{\Delta l} \tag{3.2}$$

Where subscript F is for furnace and Δl is distance between temperature measurement point and furnace. For thermal symmetry case, $T_S = T_R$, then $\Phi_{FS} = \Phi_{FR}$ is valid.

If a constant (exothermic) heat flow rate ($\Phi_r < 0$) is produced in the sample, T_S increases by ΔT_S, the temperature difference $T_F - T_S$ and thus the heat flow rate Φ_{FS} decreases. When the steady-state is reached again, for reasons of balance, the change of Φ_{FS}, ($\Delta \Phi_{FS}$), must be equal to Φ_r:

$$\Delta\Phi_{FS} = \Phi_r = -\frac{A\lambda}{\Delta l}\Delta T_S \tag{3.3}$$

On the reference sample side, there is no change, hence:

$$\Delta T_S = \Delta T_{SR} = T_S - T_R \qquad \text{and} \qquad \Phi_r = \Delta\Phi_{SR} = \Phi_{FS} - \Phi_{FR}$$

Consequently,

$$\Phi_r = -\frac{A\lambda}{\Delta l}\left(T_S - T_R\right) = -\frac{A\lambda}{\Delta l}\Delta T_{SR} = -K \cdot \Delta T \tag{3.4}$$

(Here, $T_S > T_R$, hence Φ_r is negative: exothermic effect; $\Delta T = \Delta T_{SR}$: measurement signal).

In this steady-state model, K is given by the properties of the heat conduction path between the furnace and the samples. This means that in the steady state, there is direct proportionality between the measured Φ_r and the measurement signal ΔT. The conditions of constant heat consumption can be achieved in scanning operation when the sample and the reference sample have different temperature-independent "heat capacities". A greater amount of heat will always flow into the sample whose heat capacity is higher, in order that the steady-state heating rate is maintained. With the heat capacity of sample greater than heat capacity of the reference ($C_{p,S} > C_{p,R}$), the following equation is valid for the difference between the heat flow rates to the sample and reference samples:

$$\Delta\Phi_{SR} = -K' \cdot \Delta T_{SR} \qquad \text{and} \qquad T_S < T_R \tag{3.5}$$

If there is no steady state during sample transitions or reactions, the above approximation could not apply in these cases. Furthermore, $C_{p,S}$ and $C_{p,R}$ change with temperature, but these changes are in many cases rather slow and do not affect the steady-state condition very much.

When there is a quasi-steady-state, the equation below can be used:

$$\Delta\Phi_{SR} = \beta(C_{p,S} - C_{p,R}) \qquad \text{and thus} \qquad \beta(C_{p,S} - C_{p,R}) = -K' \cdot \Delta T \tag{3.6}$$

With β is the average heating rate. Equation (3.6) is the basic equation to determine the heat capacity of a sample $C_{p,S}$. In practice, the asymmetry of the apparatus is needed to be checked first by a zero line ΔT_0 that will be recorded with both crucibles empty and subtracted from the measured curves.

In the non-steady-state process, the ΔT is not constant in time; the other assumptions are the same as for the steady-state process.

The heat capacity of a sample is shown in the equation below:

$$C_{p,S}\frac{dT_S}{dt} = \Phi_{FS} - \Phi_r \tag{3.7}$$

(exothermic: Φ_r negative, endothermic: Φ_r positive)

Where Φ_{FS} is the heat flow rate from the furnace to the sample, $\Phi_r(t)$ is the time dependent heat flow rate produced inside the sample (reaction, transition).

With $\Delta T = T_S - T_R$, Equation (3.7) becomes:

$$C_{p,S}\frac{dT_R}{dt} + C_{p,S}\frac{\Delta T}{dt} = \Phi_{FS} - \Phi_r \tag{3.8}$$

Accordingly, the following holds for the reference sample ($\Phi_r = 0$ by definition):

$$C_{p,R}\frac{dT_R}{dt} = \Phi_{FR} \tag{3.9}$$

When the difference between the two balance equations is calculated, the following is obtained:

$$\Phi_{FS} - \Phi_{FR} = \left(C_{p,S} - C_{p,R}\right)\frac{dT_R}{dt} + C_{p,S}\frac{d\Delta T}{dt} + \Phi_r \tag{3.10}$$

The following expression is valid for the heat flow rates Φ_{FS} and Φ_{FR}:

$$\Phi_{FS} = \frac{T_F - T_S}{R_{FS}} \qquad \text{and} \qquad \Phi_{FR} = \frac{T_F - T_R}{R_{FR}}$$

Where R_{FS} and R_{FR} are global heat resistances between the furnace and the samples. In the case of thermal symmetry, $R_{FS} = R_{FR} = R$, thus, Equation (3.4) becomes:

$$\Phi_r = -\frac{\Delta T}{R} - \left(C_{p,S} - C_{p,R}\right)\frac{dT_R}{dt} - C_{p,S}\frac{d\Delta T}{dt} \tag{3.11}$$

The second term takes the asymmetry of the measuring system into account as regards heat capacities of the sample and the reference sample. The third term considers the contribution of the thermal inertia of the system when a measured signal $\Delta T(t)$ appears. In analogy to the charging or discharging of a capacitor of capacity C_p, a time constant τ can similarly be defined for the heat flow rates:

$$\tau = C_{p,S} \cdot R$$

When ΔT is changed, R is the effective thermal resistance to the "charging or discharging" of the "capacity" $C_{p,S}$. With this resistance and with $dT_R/dt = \beta$, the heating rate, as the reference sample is always in a steady-state heating mode, the following results from Equation (3.5):

$$\Phi_r(t) = -\frac{\Delta T(t)}{R} - \left(C_{p,S} - C_{p,R}\right) \cdot \beta - \frac{\tau}{R} \cdot \frac{d\Delta T(t)}{dt} \tag{3.12}$$

In reality, the term $R(C_{p,S} - C_{p,R})$ reflects the temperature dependence of the thermal resistance R and of the heat capacities $C_{p,S}$ and $C_{p,R}$ causing a temperature dependences of the measured curve even without any thermal effect due to the sample.

Thus:

1. When the signal ΔT measured at a given moment is to be assigned to the heat flow rate Φ_r by which it is caused, the third term in Equation (3.12) must be taken into account. The thermal resistance R and the time constant τ must be determined by calibration.
2. For the total heat of reaction or transition Q_r developed/consumed in the sample, the following balance equation is valid:

$$Q_r = \int_{t_1}^{t_2} \Phi_r(t)dt \tag{3.13}$$

where t_1 and t_2 are the beginning and end, respectively, of the peak.

With Equation (3.12) inserted, Equation (3.13) becomes:

$$Q_r = -\frac{1}{R}\left[\int_{t_1}^{t_2} \Delta T(t)dt - \int_{t_1}^{t_2} \left(-R \cdot \Delta C \cdot \beta\right)dt\right] - \int_{t_1}^{t_2} \left(\frac{\tau}{R} \cdot \frac{d\Delta T}{dt}\right)dt \tag{3.14}$$

3. For the partial integration of the peak between t_1 and t^*, the contribution of the 3rd term must be taken into account at the point t^*

$$Q_r = -\frac{1}{R}\left[\int_{t_1}^{t^*} \Delta T(t)dt - \int_{t_1}^{t^*} \left(-R \cdot \Delta C \cdot \beta\right)dt\right] - \int_{t_1}^{t^*} \left(\frac{\tau}{R} \cdot \frac{d\Delta T}{dt}\right)dt \tag{3.15}$$

The partial integrations of peaks are necessary for kinetic investigations and to determine the purity of a substance.

3.1.1.3 – Application:

Differential Scanning Calorimetry is the most widely used thermal technique in the study of liquid crystals, oxidative stability, drug analysis, food science, and polymers[41-45]. From the DSC output signals, the heat flow rate as a function of temperature, and any derived quantity, such as the heat of transformation or reaction, or any change of the heat capacity of the sample can be used to understand the properties of a substance.

Different instrument manufactures, such as Netzsch Instruments, Setaram Instrumentation, PerkinElmer Instruments, TA Instruments, and Mettler Toledo offer different type of DSC and thermal analysis instruments depending on the research. The DSC used in this study is Setaram TG – DSC 111, which is a heat-flux DSC.

3.1.2 – Temperature Modulated Differential Scanning Calorimeter

3.1.2.1 – Technique Overview

Differential scanning calorimetry (DSC) involves heating and cooling a sample at a constant rate. This technique was established during the 1960s and remained unchanged for almost three decades. During 1990's, a new technique, temperature modulated differential scanning calorimeter (TMDSC) was developed. The concept behind TMDSC has been around since the early 1910[46, 47], although no concrete model existed at the time. Gobrecht et al.[48] first introduced a model for TMDSC and cited several technical limitations. In 1993, the concept was reintroduced by Reading, who had overcome the limitations observed by Gobrecht.

The basic principle behind TMDSC is quite simple. A constant heating rate, similar to the one used in conventional DSC, is modulated by superimposing upon it a periodic temperature modulation of a certain amplitude and frequency. This results in a simultaneous introduction of two different time scales in the experiment: a long time scale corresponding to the underlying heating rate, and a shorter time scale (or cycle) corresponding to the period of the modulation[49]. Figure 3-1 illustrates an example of

temperature modulation as a function of time with a modulated heating rate represented by a blue line.

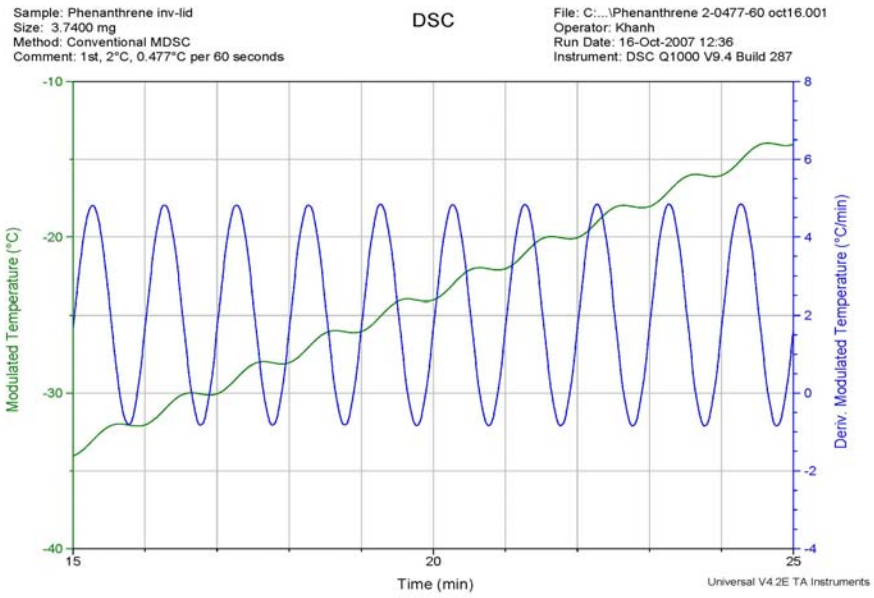

Figure 3-1: Modulated temperature profile as a function of time

3.1.2.2 – Theory:

The most common TMDSC data analysis involves separating the total heat flow or apparent heat capacity into reversing and non-reversing components; this method was first suggested by Reading et al.[50, 51] The normal response of DSC under a condition where no significant temperature gradient exists in the sample is a combination of a signal that is dependent on the absolute value of the temperature as this will govern the rate of any kinetically driven process.

$$\frac{dQ}{dt} = C_{p,t}\frac{dT}{dt} + f(t,T) \tag{3.16}$$

where Q is the amount of heat absorbed by the sample, $C_{p,t}$ is the thermodynamic heat capacity at constant pressure and time related to the energy stored in the vibration, rotation, and translational motion of the sample, T is the absolute temperature, t is the time, and $f(t,T)$ is some function of time and temperature that governs the kinetic response of any physical or chemical transformation.

In TMDSC, the temperature program consists of an underlying trend that is modulated by a small perturbation. The underlying trend is usually the conventional linear temperature rise with time. A periodic temperature at a single frequency is superimposed on a linear temperature time profile given by[50, 51]:

$$T(t) = T_0 + q_0 t + A_T \sin(\omega \cdot t) \tag{3.17}$$

where q_0 is the underlying heating/cooling rate, A_T *and* ω are the amplitude and frequency of the temperature modulation, respectively. $T(t)$ and T_0 are the temperature of the sample at time t and at time $t = 0$ when the sample follows the applied furnace temperature.

With the assumption that temperature modulation is small over the interval of the modulation, the response of the rate of the kinetic process to temperature can be approximated as linear. Derivative of Equation (3.17) is derived as follows:

$$q(t) = \frac{dT(t)}{dt} = q_0 + \omega A_T \cos(\omega \cdot t) \tag{3.18}$$

The heating rate fluctuates between a maximum $(q_0 + \omega A_T)$ and a minimum $(q_0 - \omega A_T)$ value and, depending on the magnitude of the three measuring parameters q_0, A_T, and ω, different modes of TMDSC operation can be distinguished

- quasi-isothermal mode: $q_0 = 0$
- heating only mode: $\omega A_T < q_0$
- heating-iso mode: $\omega A_T = q_0$
- heating cooling mode: $\omega A_T > q_0$

All these modes are used in practice, often without consideration about possible consequences concerning the result of the measurements, which may be different depending on the sample and processes in question. However, there are different temperatures and different temperature fluctuations as well as different heating rates during the TMDSC run, and such processes which react either to temperature or to heating rate changes will give different signals.

Equation (3.16) can be rewritten as:

$$\frac{dQ}{dt} = C_{p,t}\left[q_0 + \omega A_T \cos(\omega \cdot t)\right] + f^{'}(t,T) + C\sin(\omega \cdot t) \qquad (3.19)$$

Where $f^{'}(t,T)$ is the underlying kinetic function once the effect of the sine wave modulation has been subtracted and C is the amplitude of kinetic response to the sine wave modulation. The heat flow signal contains a cyclic component that depends on the values of A_T, ω, and C. The kinetic contribution $f^{'}(t,T) + C\sin(\omega \cdot t)$ occurs only during irreversible processes, while the heat capacity contribution $C_{p,t}\left(q_0 + \omega A_T \cos(\omega \cdot t)\right)$ is always present. For many kinetically controlled processes, C may be approximated to zero such that the response to the cyclic perturbation originates from the thermodynamic heat capacity contribution alone.

A discrete Fourier transform is used to separate the modulated heat flow component from the underlying heat flow signal. The modulated heat flow component is termed the reversing (or $C_{p,t}$) component. The non-reversing (kinetic) heat flow component is the obtained by subtraction of the reversing component from the calculated total heat flow.

Figure 3-2 illustrates total, reversing, and non-reversing heat flow signals for a sample undergoing endothermic and exothermic transitions.

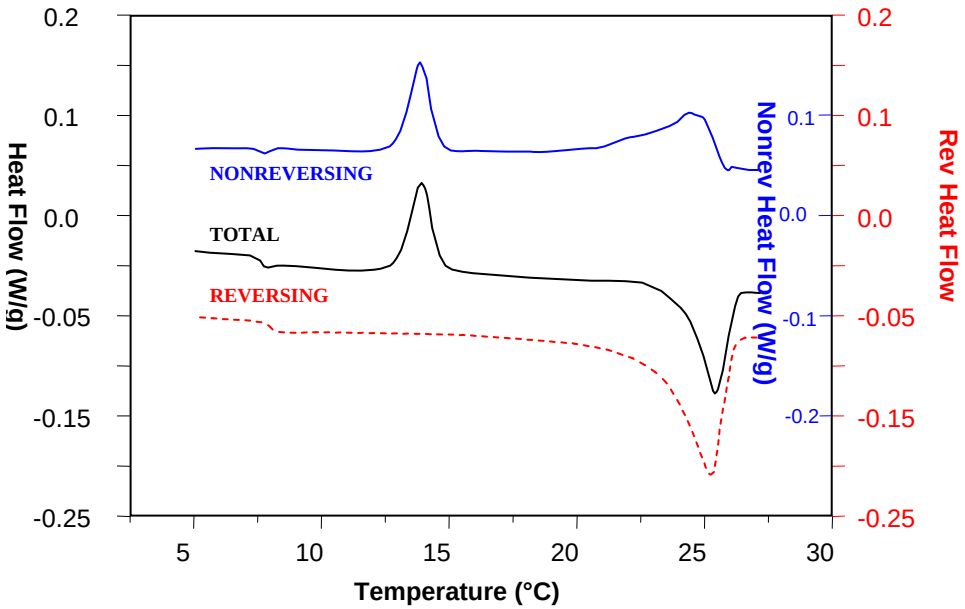

Figure 3-2: The output signals from TMDSC

Another approach to treat data from TMDSC was suggested by Reading and colleagues[51-54] and Schawe[55]. It considers the periodic part of the response only and describes the measured heat capacity as a complex value.

$$C_p^* = C_p^{'} - iC_p^{''} \tag{3.20}$$

where $C_P^{'}$ and $C_P^{''}$ are the real and imaginary part of the complex heat capacity, respectively.

$$C_p^{'} = \mid C_p^* \mid \cos\delta_s \tag{3.21}$$

$$C_p^{''} = \mid C_p^* \mid \sin\delta_s \tag{3.22}$$

Here δ is the phase angle between the sinusoidal heat flow and the sinusoidal heating rate. This approach is only valid if the response is linear[55]. The existence of a complex heat capacity has been based on the dissipation theory[56].

3.1.2.3 – Application:

TMDSC has been used to study the melting, glass transition, crystallization, absolute heat capacity, etc.[57-69] The study of glass transitions is one of the most successful applications of TMDSC.[63, 64, 70] TMDSC allows the study of weak glass transitions, which are typically difficult to observe in conventional DSC; also the variation of the modulation frequency allows for an independent study of the dynamics of glass transition. In some cases, glass transitions superimposed with truly non-reversing events like evaporation, cold crystallization, or curing can be detected in the multi components heat capacity.

TMDSC is commercially available from different instrument manufacturers, which use their own trade names, such as: TA Instruments – MDSC™, PerkinElmer Instrument – DDSC™, StepScan™ DSC, Mettler Toledo – ADSC™, Seiko – ODSC™, each of which offered slightly different modulated temperature profiles and slightly different procedures for analysis of the data[49]. The TMDSC used in this study is TA Instruments Q1000 DSC, which includes the modulate mode.

DSC Advantages – TMDSC Limitations:

The maximum heating rate of DSC (approximate 20 K/min) is relatively fast compared to TMDSC (approximate 3 K/min). DSC provides a single heat flow signal and requires only a few experimental parameters. On the other hand, TMDSC generally uses three heat flow rate signals but more than ten are available; furthermore, TMDSC requires additional experimental parameters, modulation period, and temperature modulation amplitude.

DSC Limitations – TMDSC Advantages:

DSC measures only the sum of all thermal events occurring at a specific temperature or time during the experiment. This often causes difficulty in detection of small transitions or in data interpretation. TMDSC improves upon conventional DSC since it measures the total, reversing, and non-reversing heat flow rate signals. Its ability to resolve complex transition into specific components improves data interpretation.

The only way to improve sensitivity for detecting low energy transitions is to increase sample size and/or heating rate. This however decreases resolution. Thus, it is not possible to optimize sensitivity and resolution in a single DSC experiment with a single heating rate. TMDSC has two independent heating rates. The average rate can be as low as necessary to achieve the desired resolution while the modulated rate can be kept high to maintain sensitivity.

The absolute value of the DSC heat flow signal is affected by instability in instrument electronics and cooling system, and environmental changes such as temperature and humidity in the surrounding. This limits the sensitivity to small transitions in DSC as required by a straightness of the baseline. TMDSC greatly improves interpretation because overlapping transitions can be separated into different signals while multiple transitions can occur in the same temperature range in DSC.

It is recommended that getting the benefits of DSC by first characterizing new samples with conventional DSC and then switching to TMDSC when one needs any of its advantages.

3.2 – Instrument Description

3.2.1 – TA Instrument Q1000 DSC (TMDSC)

The Temperature Modulated Differential Scanning Calorimeter used in this study is TA Instrument Q1000 DSC, as seen in Figure 3-3. It is top of the line from TA Instrument; it contains advanced Tzero technology. Q1000 DSC is considered a research-grade DSC, with unmatched performance in baseline stability, sensitivity, and resolution. Its features include Modulated DSC, a 50-position intelligent auto-sampler, and digital mass flow controllers. Q1000 DSC can perform within the temperature range of 93 K to 998 K (-180°C to 725°C) with a suitable cooling accessory.

Figure 3-4 illustrates the Tzero sensor of Q1000 DSC; it is designed for excellence in both heating and cooling operations. It has been innovated from Q100 DSC; many innovations include a new sensor with raised sample and references platforms. The sensor is machined for symmetry from a single piece of durable, thin wall, high response constantan and brazed to the silver heating block. Also, the innovated Tzero cell provides faster signal response, flat baselines, superior sensitivity and resolution, plus improve data precision. The auto lid assembly that consists of dual silver lids and a dome-shaped heat shield provides more accurate measurements result from improved thermal isolation of the cell.

The innovation design features an array of 54 symmetrically arranged with high conductivity nickel cooling rods that connect the silver furnace with the cooling ring provides superior cooling performance over a wide temperature range, as seen in Figure 3-5. This improvement helps to achieve high heating rate and the instant switching from heating to cooling. Lower sub-ambient temperatures and unmatched baseline performance can now be obtained with the range of cooling accessories in isothermal, programmed cooling, and MDSC experiments. Turnaround time between experiments is significantly reduced.

Figure 3-3: TA Instrument Q1000 DSC

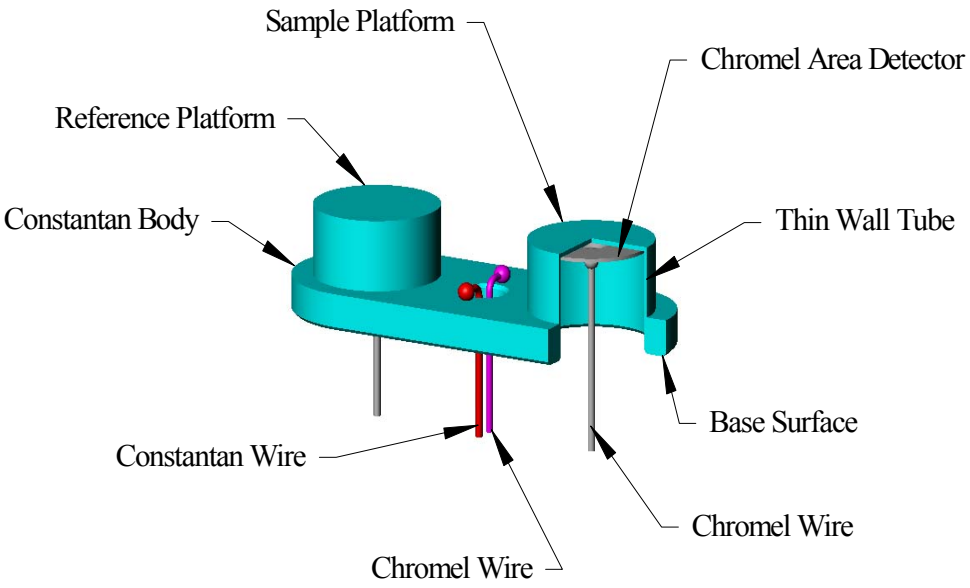

Figure 3-4: Tzero Cell Design of TA Q1000 DSC

The sample and reference platforms are surrounded by a high thermal conductivity, silver furnace, which uses rugged, long-life Platinel windings. Purge gases area accurately and precisely metered by mass flow controllers and uniformly heated to cell temperature, prior to introduction to the sample chamber. This design provides a highly uniform

thermal environment for the sample and reference. Precise temperature control algorithms deliver accurate isothermal temperatures, linear heating rates, rapid temperature response and the ability to heat at rates up to 200 K/min. The rugged heater windings ensure long furnace life. Superior data quality results from the uniform purge gas flow.

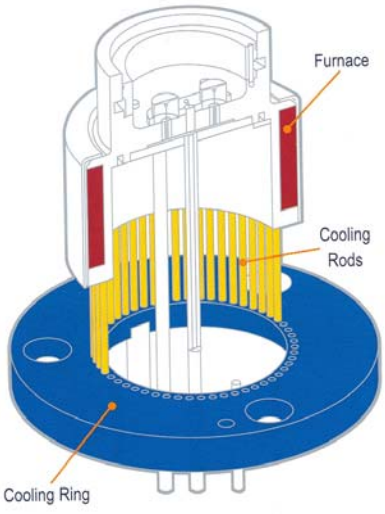

Figure 3-5: The connection between furnace and cooling rods and ring in TMDSC

There are three cooling systems that can be used with Q1000 DSC, such as refrigeration, liquid nitrogen, air, and quench; the refrigerated cooling system (RCS) and liquid nitrogen cooling system (LNCS) are the most common used in the laboratory. The RCS can be operated from 183 to 823 K using a two-stage, closed, evaporative refrigerator system. It is frequently selected as the cooling device of choice for trouble-free, unattended DSC and MDSC operation. The LNCS provides the highest performance and greatest flexibility in cooling. The operating temperature range with LNCS is 93 to 823 K with a greatest cooling rate capacity, which is up to 140 K/min; it is ideal for isothermal crystallization studies. The finned air cooling system (FACS) uses compressed air to cool the DSC cell. The operating temperature range is between ambient and 998 K. It can be used for controlled cooling experiments, thermal cycling studies, and to improve sample turnaround time. The FACS offers a cost-effective alternative to the refrigerated and liquid nitrogen.

3.2.2 – Setaram TG – DSC 111

The TG – DSC 111 thermo-analyzer from Setaram contains the CS 32 processing unit and the assembly coupling the B111 microbalance to the DSC 111 calorimeter. The CS 32 controller is essentially made up of a CPU card, a power supply card, a balance card, amplification card for calorimetric signal, temperature acquisition card for temperature measurement, and temperature acquisition card for temperature regulation.

The B111 electronic microbalance is a beam balance articulated on a torsion band held under load between two springs. The proportional relationship linking the current to the force of electromagnetic equilibrium combines measuring the current variations with measuring the variations in mass. A potential difference proportional to the equilibrium current is amplified and is available for digital use in the CS 32 controller.

The DSC 111 calorimeter contains calorimetric transducer, a junction box, and the pre-amplification and amplification cards for the DSC signal. The calorimetric transducer is shaped like a rectangular parallelepiped. Two sintered alumina tubes with an inner diameter of 7 mm cross the chamber from side to side. The bore of the tubes has no restrictions and enables a sample to move from one end to the other. Both tubes are parallel and set symmetrically in the chamber with a centre-line to centre-line distance of 17 mm. The sensitive part in the calorimeter is the central area in each of the tubes. The heart of the calorimetric block contains two cavities in which are set the thermocouple-carrying heat-flux transducers wrap around the central part of the tubes. The heat passed on by the system under study, in connection with the calorimetric block, transits via the thermocouple-carrying heat-flux transducers and thus can be measured accurately and reliably. This measurement is independent of the sample's exact shape as well as of the flow, of the pressure and the nature of the gas present in the tube.

The symmetrical arrangement of the transducer provides cancellation of the signal resulting from the two heat-flux transducers being set in opposition, when the two samples are themselves identical regardless the thermal state of the calorimeter. The

working signal only contains the "differential" component in the properties of an active sample placed in one of the tubes and of a "reference" placed in the other tubes.

On the front panel of the working chamber, a part is designed to take pipe-work carrying the refrigerant used for cooling the calorimeter.

3.3 – Sample Preparation

The reference samples used in this study were hexadecane, phenanthrene, and powdered polystyrene with an average molecular weight of 400,000 g/mol. All the reference samples were obtained from Sigma Aldrich.

Asphaltenes were precipitated from Athabasca bitumen, at room temperature and atmospheric pressure, by addition of *n*-alkane to crude oil using a solvent/oil ratio of 40[11, 29, 34]. The asphaltenes precipitation procedure was the same for each of the *n*-alkane used (C_5, C_6, C_7, C_8, C_9, C_{10}, C_{11} and C_{12}). A sample of crude oil was mixed with the solvent in a flask keeping a solvent/oil ratio of 40 ml/g. The solution was stirred overnight at room temperature. Afterward, the mixture of *n*-alkane and oil was filtered in two steps using a vacuum system. First, the solution was filtered through a Fisher brand filter paper Q2, with a pore size between 1-5 μm. Then, permeate was filtered using a 0.22 μm Millipore membrane (mix cellulose ester). The filtration membranes and the flask were washed with small volumes of the corresponding *n*-alkane in order to eliminate any residual oil. The membranes were washed until the filtrate (permeate) was colorless. The membranes with the precipitated material were dried at 373 K for 30 minutes and afterward they were placed overnight in a vacuum oven at approximate 10 kPa. Finally, the filtered samples were weighted in order to determine the amount of asphaltene precipitated as a fraction of the original sample.

3.4 – Experimental Procedure

3.4.1 – Differential Scanning Calorimetry

A differential scanning calorimeter Setaram TG – DSC 111 was used for heat capacity measurements in the temperature interval of 210 K and 523 K. The measurements were carried out with a heating rate of 5 K/min with isothermal periods of 20 minutes at the beginning and the end of each experiment. The experiment was repeated with the same sample with a cooling rate approximate 10 K/min. The typical mass of samples used was about 50 mg (uncertainty in mass was 0.05 mg). The operating principle for TG – DSC 111 was Tian – Calvet principle. The three-step procedure was used for DSC measurements to obtain heat capacity values. The measuring cell was empty in the first run and filled with the reference material (synthetic sapphire) and the measured sample in the second and third runs, respectively. The reference cell was empty during all runs. Hermetically sealed cells were utilized in all experiments with a maximum pressure of 10 MPa at 573 K. The tightness of the cells was checked using naphthalene where no mass loss was detected following exposure to 700 K. The vapor pressure of naphthalene at 700 K is 1.8 MPa. The cells were weighed prior to and after each trial. No mass loss of the samples was detected[11, 29].

The heat capacity of the sample was calculated using the software provided for the instrument. The collected signals from DSC included heat flow in J/g, temperature in Kelvin, time in seconds, and heat capacity in J/(g·K).

3.4.2 – Temperature Modulated Differential Scanning Calorimetry

All experiments were performed using a TA Instruments Q1000 DSC with RCS mechanical cooling system. The experiment conditions (pan type, modulate amplitude, and period) for samples are similar as for TMDSC heat capacity calibration. A 2 – 5 mg of sample was encapsulated in hermetically sealed aluminum pans with inverted lids. DSC cell was purged with nitrogen. Thermal program comprised: equilibration at 193 K,

modulation ± 0.48 K every 60 seconds, and temperature ramp 2 K/min to 523 K. The sample was held isothermal for 15 minutes before and after heating. The experiment was repeated with the same sample with a cooling rate approximate 10 K/min. The reproducibility was also tested.

There were 15 signals collected during an experiment, including time, temperature, heat flows and heat capacities (total, reversing, and non-reversing), temperature amplitude, heat flow amplitude, heat flow phase, modulated temperature, modulated heat flow, reference sine angle, and sample purge flow. The data was exported into Microsoft Excel for the further analysis.

Furthermore, Thermogravimetric analysis (TGA) was carried out using TA Instrument Q500 Thermogravimetric Analyzer (TGA) to study the decomposition of approximate 10 mg pentane asphaltene sample from room temperature up to 573 K.

3.5 – Calibration

3.5.1 – Differential Scanning Calorimeter

The working group "Calibration of Scanning Calorimeters" of the German Society of Thermal Analysis (GEFTA)[71-74] recommended the calibrations for the DSC calorimeter. The temperature calibration to ITS 90 was performed using indium (NIST standard reference material 2232), tin (NIST SRM 2220), lead and aluminum. Energy calibration was performed using the Joule effect method in the factory and checked by measuring the heat of fusion of naphthalene, which was a primary reference material for the heat of fusion measurements recommended by ICTAC[75], and phenanthrene. The agreement with recommended literature values[75-77] was within 2%. Heat capacity *Cp* (heat flux) calibration was performed using synthetic sapphire, which was a primary reference material according to NIST (SRM 720) and ICTAC, and naphthalene, a secondary reference material for *Cp* measurements recommended by ICTAC[75]. The uncertainty of *Cp* measurements using the continuous method was estimated to be less than 4% (0.05 J/(K·g)) in the temperature range from 210 K to 300 K, where the cooling unit with liquid

nitrogen is used, and less than 2 % (0.02 J/g/K) in the temperature range from 300 K to 560 K.

3.5.2 – Temperature Modulated Differential Scanning Calorimeter

The Modulated DSC (MDSC) heat capacity calibration is required to measure the absolute value of the sample's heat capacity and it is required to perform after the DSC Tzero calibration. Sapphire was used to perform this calibration. The aluminum pans were used for this experiment. The lids of the hermetically sealed pans were inverted to minimize the thermal gradients and provide a more accurate measurement of heat capacity. Thermal program for MDSC heat capacity calibration contained zero heat flow at 383 K, equilibrated at 193 K, modulated ± 0.47 K every 60 seconds, kept isothermal for 15 minutes, then ramped 5 K/min to 573 K. After the calibration experiment was completed, the following formulas were used to calculate the heat capacity calibration factor for each signal:

$$K_{Cp}\ (\text{Total}) = \text{Theoretical value}/\ \text{Measured value}$$

$$K_{Cp}\ (\text{Reversing}) = \text{Theoretical value}/\ \text{Measured value}$$

The calibration factors were entered into the Cell/Temperature Table in the instrument control software before performing experiments with other samples.

DSC Tzero calibration (including cell resistance & capacitance, cell constant, and temperature calibration) was required. Cell resistance & capacitance was calibrated at a heating rate of 20 K/min between 183 K and 673 K with empty and sapphire; the cell constant and temperature calibration was done with indium at heating rate of 10 K/min between 373 K and 453 K. This agrees with the reference sample for temperature calibration and heat capacity calibration within 5%.

3.6 – Data Analysis

Lastovka et al.[11, 12] provided a generalized correlation for the specific heat capacity of organic solids based on elemental composition. They suggested that the predictive

correlation can be applied to a broad range of compounds from 50 K to the first transition temperature. Their expression for solid state heat capacity is:

$$C_P = 3\left(A_1\alpha + A_2\alpha^2\right)R\left(\frac{\theta}{T}\right)^2 \frac{\exp\left(\frac{\theta}{T}\right)}{\left[\exp\left(\frac{\theta}{T}\right)-1\right]^2} + \left(C_1\alpha + C_2\alpha^2\right)T + \left(D_1\alpha + D_2\alpha^2\right)T^2 \qquad (3.23)$$

where T is temperature in Kelvin. The coefficients ($A_1 = 1.3183 \cdot 10^{-2}$, $A_2 = 2.4938 \cdot 10^{-1}$, $C_1 = 2.6526 \cdot 10^{-2}$, $C_2 = -2.4942 \cdot 10^{-2}$, $D_1 = 2.500 \cdot 10^{-5}$, $D_2 = -1.2300 \cdot 10^{-4}$, and $\theta = 151.867$) are universal constants. R is the universal gas constant (8.3145 J/(K·mol)), and α can be evaluated from elemental composition as follows:

$$\alpha = \frac{N}{M} = \frac{\sum_{i=1}^{n} v_i}{\sum_{i=1}^{n} v_i M_i} = \frac{\sum_{i=1}^{n} x_i}{\sum_{i=1}^{n} x_i M_i} = \frac{\sum_{i=1}^{n} \frac{w_i}{M_i}}{\sum_{i=1}^{n} w_i} \qquad (3.24)$$

In Equation (3.24), v_i is the stoichiometric coefficient for element i in a compound consisting of N atoms, n is the number of elements in a compound, and M_i is the molar mass of chemical element i (g/mol). Variable x_i and w_i are the mole and mass fraction of element i in a compound, respectively.

The principal applications for this correlation is the provision of an accurate and consistent baseline for measurements performed in this study as the correlation is ideally suited for specific heat capacity estimation and phase transition identification for poorly defined mixed organic solids such as asphaltenes, where elemental analysis is available but not molecular structure.

Reference samples:

The properties of the reference samples are listed in Table 3-1.

Table 3-1: Properties for reference samples used in this study

	Hexadecane	Phenanthrene	Polystyrene
Formula	$C_{16}H_{34}$	$C_{14}H_{10}$	$(C_8H_8)n$
Purity	99%	99%	--
Molar mass	226.44	178.23	400,000
Boiling point (K)	554±10	609.15	--
Melting point (K)	291±1	372±2	--
ΔfusH (kJ/mol)	292.1	--	--

Hexadecane and polystyrene were only measured with TMDSC; however phenanthrene was measured with both DSC and TMDSC. The measured total heat capacity was corrected by adding offset value based on the data obtained from the literature and DSC. The literature heat capacity for phenanthrene was obtained from the following equations.

$$Cp = A + BT + CT^2 + DT^3 + ET^4 \tag{3.25}$$

where T is temperature in Kelvin, A, B, C, D, and E are constant coefficients depending on temperature range and showed in Table 3-2.

Table 3-2: Constant coefficients for heat capacity equation of phenanthrene obtained from literature

	A	*B*	*C*	*D*	*E*
Crystal III (20 to 270 K)	-6759.1	1376	-9.0217	0.040749	-6.03E-05
Crystal II (270 to 342.23 K)	-1.49E+07	152290	-514.82	0.58299	--
Crystal I (347.5 to 372.39 K)	223630	-196.3	0.96	--	--
Liquid (372.39 to 500 K)	103370	527.03	--	--	--

The reversing heat capacity of phenanthrene was obtained from TMDSC measurements and corrected at lower temperature (193 K to 273 K) with the literature values. Non-reversing heat capacity was obtained from the difference between total and reversing heat capacities.

Asphaltene samples:

In this study, the specific heat capacity equation from Lastovka et al.[11, 12] was used as the predicted specific heat capacity for the compounds for which there are no specific heat capacity data in the literature. For the asphaltene samples, elemental compositions for Athabasca bitumen asphaltenes were obtained in Table 3-3.

Table 3-3: Elemental compositions for Athabasca asphaltenes[11, 12]

Sample	α (mol/g)	Mass fraction (wt%)				
		C	H	N	O	S
Athabasca asphaltenes	0.151	80.84	7.99	1.27	2.43	7.47

The total apparent heat capacities of asphaltene samples from 210 K to 573 K were obtained from Setaram TG - DSC 111 and the reversing heat capacity data were collected from TA Instrument Q1000 DSC (TMDSC). Due to the offset of reversing heat capacity, reversing heat capacity was corrected at low temperature (193 K to 273 K) with the predicted heat capacity from Lastovka et al.[11] The correction was valid since there was no difference between total and reversing heat capacity at low temperature, where the samples were still in the solid state (no kinetic event happened). Non-reversing heat capacity of the samples was calculated from the difference between total and reversing heat capacities.

CHAPTER 4 - RESULTS AND DISCUSSION

4.1 – Reference Samples

Hexadecane:

Hexadecane was used to illustrate a solid to liquid phase transition with TMDSC. Figure 4-1 illustrates three heat capacity components for hexadecane obtained at a heating rate of 3 K/min using the TA Universal Analysis program; the enthalpies of fusion for three heat capacity components are also indicated.

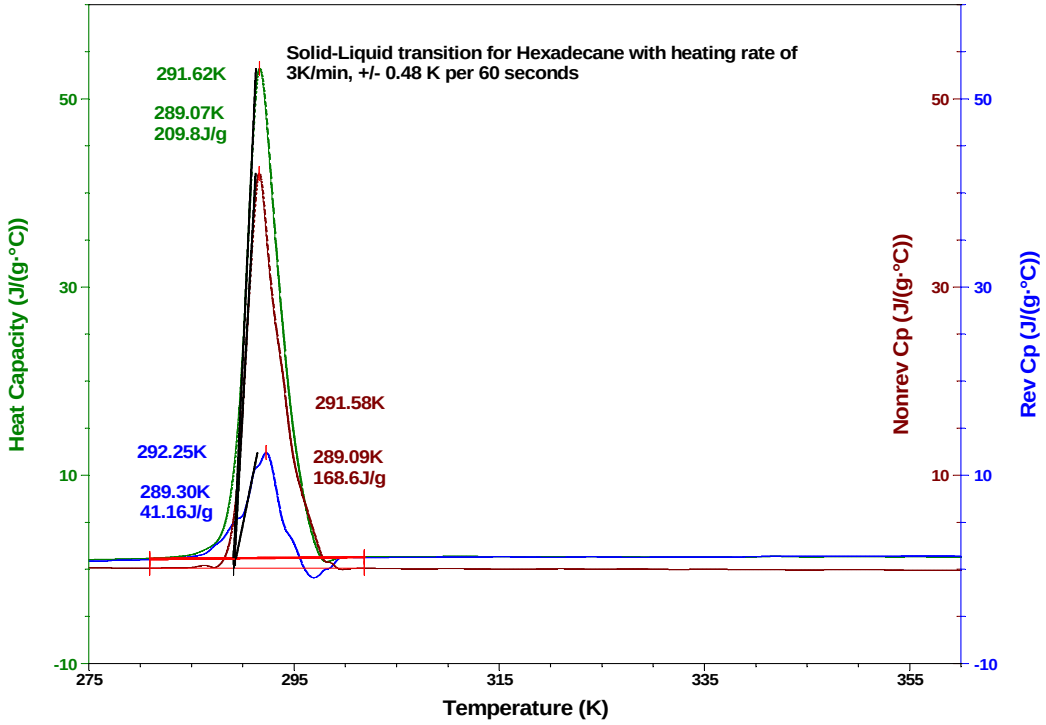

Figure 4-1: Total, Reversing, and Non-reversing heat capacities for hexadecane obtained from TMDSC with a heating rate of 3 K/min and an amplitude of 0.48 K for a 60 second period

Table 4-1 shows a comparison between enthalpy of fusion values for hexadecane in the literature obtained from the calorimetric methods and measurements in the present work, noting that only the enthalpy of transition for total heat capacity was used. The measured enthalpy of transition for a heating rate of 3 K/min agrees with the values obtained by

Claudy and Letoffe in 1991 within ±0.2 J/g; but it is lower compared to others. On the other hand, the measured melting temperature of hexadecane agrees with the literature within ± 1 K, which is within 5% error of the measured experiment.

Table 4-1: Enthalpy of fusion for Hexadecane obtained from NIST database and TMDSC

	ΔH_{fusion} (J/g)	Temperature (K)
Claudy and Letoffe, 1991	209.966	292.1
Finke, Gross, et al., 1954	235.642	291.34
Parks, Moore, et al., 1949	227.622	291.1
TMDSC (3 K/min) this work	209.8	291.62

Phenanthrene:

Phenanthrene exhibits a second order solid transition (crystal III to crystal II), a first order solid transition (crystal II to crystal I), and solid – liquid transition[77] and is also used as a reference sample for DSC and TMDSC measurements in this study. Figure 4-2 illustrates the total, reversing, and non-reversing heat capacities for phenanthrene obtained from the TMDSC. The enthalpies of transition in three components were also included.

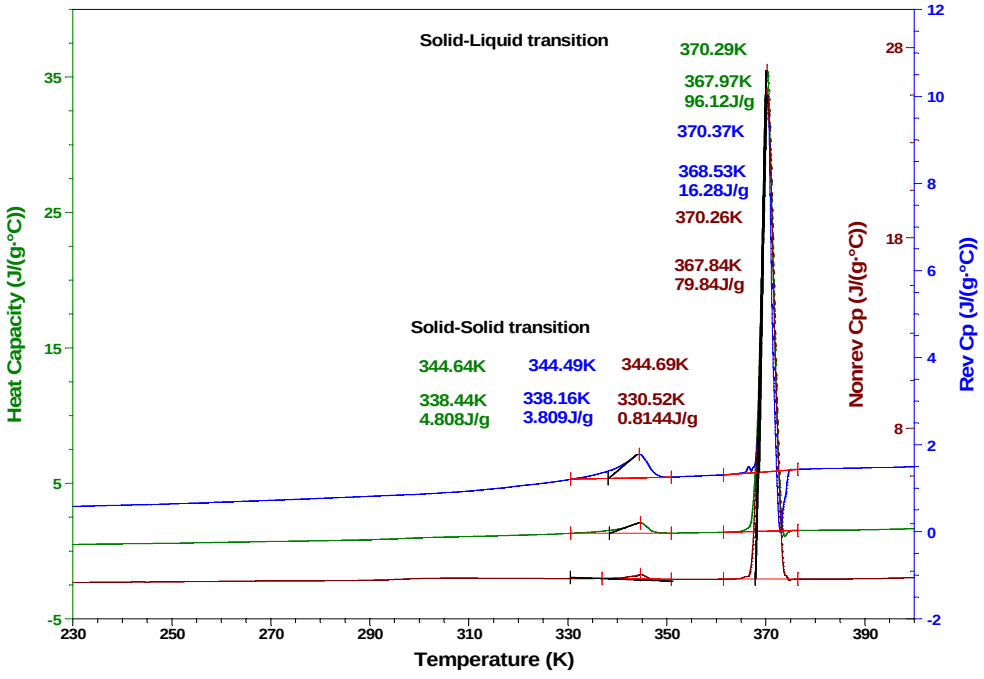

Figure 4-2: Three heat capacities signals obtained from TMDSC for phenanthrene with a heating rate of 2 K/min, an amplitude of 0.48 K per 60 seconds period

Table 4-2: Enthalpy of transitions for phenanthrene obtained from NIST data base and TMDSC

	Crystal II → Crystal I		Crystal I → Liquid	
	$\Delta H_{transition}$ (J/g)	T (K)	$\Delta H_{transition}$ (J/g)	T (K)
Sabbah and El Watik, 1992	--	--	88.201	373.8
Petropavlov, Tsygankova, et al., 1988	5.611	332.2	--	--
Rai, Singh, et al. 1987	--	--	104.512	373
Finke, Messerly, et al. 1977	1.223	347.5	92.370	372.4
Rastogi and Bassi, 1964	--	--	100.994	373.2
Ueberreiter and Orthmann, 1950	14.588	342	104.472	373
Eibert, 1944	--	--	96.225	371.4
Schmidt, 1941	--	--	96.157	371.7
Lastovka, Fulem, Becerra, Shaw, 2008[11] (DSC, 5 K/min)	4.70±0.2	347.8±0.5	89.6±1.8	375.7
TMDSC (2K/min, ±0.48K per 60 sec)	4.808	344.6	96.12	370.3

A comparison for enthalpy of transition between measured and literature values are presented in Table 4-2. From Table 4-2, it is observed that the temperature for crystal II-crystal I transition varies from 332.2 K to 347.5 K; but it is in the range of 371 K to 374 K for the transition from crystal I to liquid. The enthalpy of transition in the literature ranges from 1.223 J/g and 14.588 J/g for crystal II to crystal I and from 88.201 J/g to 104.472 J/g for transition from crystal I to liquid. It can be seen that there is no agreement in literature regarding the temperature and enthalpy of transition for first order solid transition (crystal II to crystal I); it could be due to the difference in temperature interval chosen for integration. On the other hand, the data obtained from Lastovka et al.[11] with DSC agree with measured data from TMDSC within experimental error for the first order solid transition in phenanthrene. For the solid-liquid transition, the temperature and enthalpy of transition obtained from both DSC and TMDSC are within the range reported in the literature.

Figure 4-3 shows the heat capacities regressed from the literature using Equation (3.25), predicted values based on Equation (3.23), DSC experimental results, and TMDSC experimental results. A crystal II – crystal I transition and crystal I - liquid transition is identified by both DSC and TMDSC. However, the total heat capacity obtained from TMDSC is higher than the values from DSC at the melting region of the sample. Total heat capacities obtained from TMDSC measurements are not quantitative.

As reported in the literature, phenanthrene exhibits a second order solid transition (crystal III to crystal II) in the temperature range 270 K – 280 K[11, 77]. Neither DSC nor TMDSC detects this solid-solid transition and there is no record for the enthalpy of transition of this solid-solid transition in the NIST data bank. Using Equation (3.25), the energy of second order solid transition for phenanthrene is calculated to be 0.00989 J/g with the temperature interval of 10 K. Such a small transition is below the detection limits of both DSC and TMDSC.

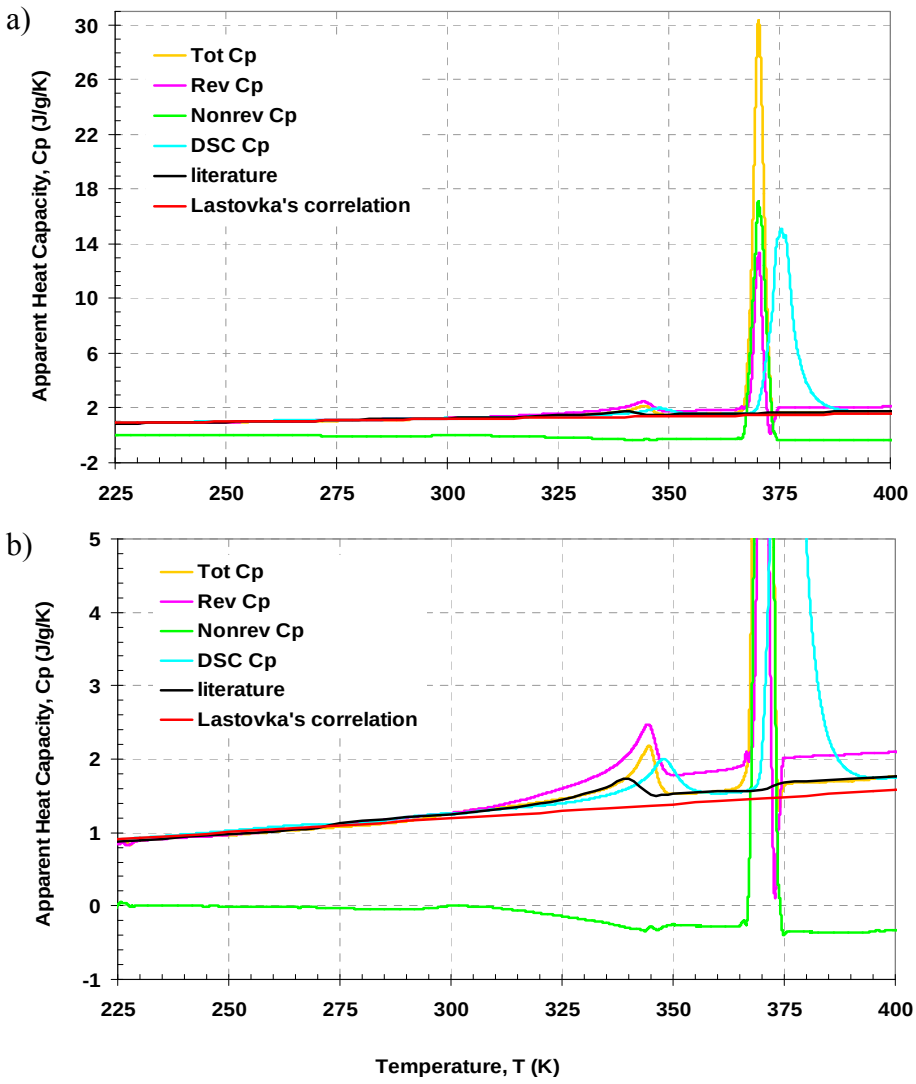

Figure 4-3: Literature and apparent heat capacities of phenanthrene obtained from TMDSC and DSC; a) solid-liquid transition, b) solid-solid transition

Polystyrene:

Polystyrene is a widely used reference polymer[63, 66, 70, 78, 79]; the purpose of using polystyrene in this study is comparing the glass transition temperature reported from the literature and measured values obtained from TMDSC. Figure 4-4 illustrates the first heating cycle result for polystyrene obtained using TMDSC with a heating rate of 2 K/min and amplitude of 0.48 K per 60 seconds period. The results were plotted using the Universal TA Instrument program. The enthalpies of transition for three components (total, reversing, non-reversing) are also presented. From Figure 4-4, the glass transition can be observed through total, reversing, and non-reversing heat capacities. After cooling back to the start temperature with a cooling rate of 15 K/min, the same sample of polystyrene was reheated to 420 K. The repeatability of the polystyrene measurement is illustrated in Figure 4-5. The results of three heating experiments agree with each other within the experimental error for total, reversing, and non-reversing heat capacities. The glass transition for polystyrene was also evaluated using the quasi-isothermal TMDSC mode with an increment of 2 K and amplitude of 0.48 K per 100 seconds from 300 K to 420 K. Again, total heat capacity is not quantitative.

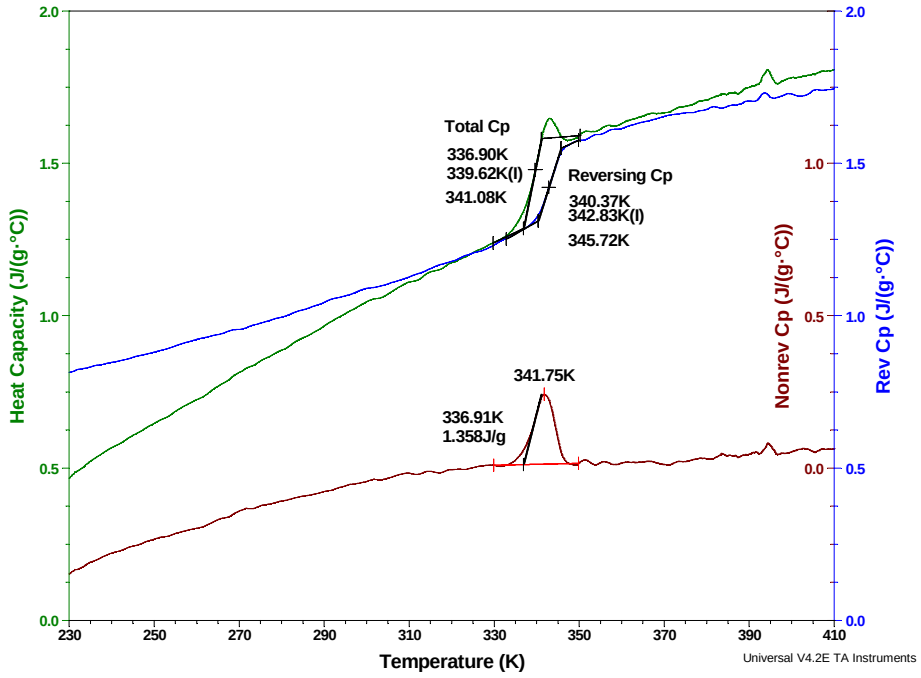

Figure 4-4: TMDSC heat capacity signals for 3.16 mg polystyrene MW 400,000 g/mol

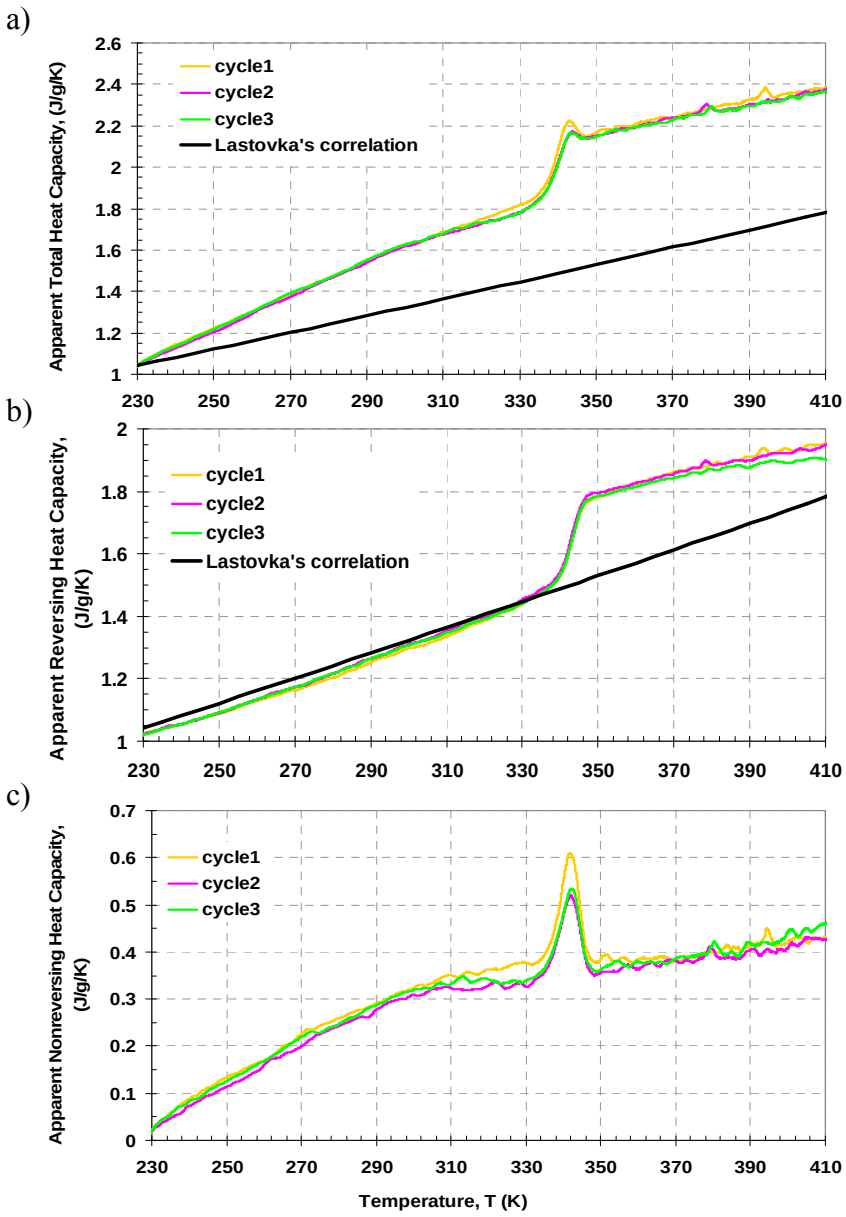

Figure 4-5: Reproducibility of TMDSC for polystyrene in a) total, b) reversing, and c) non-reversing heat capacities

Xu et al.[65, 66] used conventional DSC and quasi-isothermal TMDSC to study the heat capacity of solution grown crystals of isotactic polystyrene from below the glass transition temperature (T_g) and above the melting. Xu et al.[65, 66] found that the T_g for bulk isotactic polystyrene (iso-PS) was at 377 K with an error of ±0.5 K with a heating rate of 10 K/min. However, Koh et al.[79] found that the T_g for bulk polystyrene was approximately 372.25 K. Koh et al.[79] studied the glass transition and absolute heat

capacity of ultra thin polystyrene films with DSC using the step-scan method (heating rate of 10 K/min). Fakhraai and Forrest[78] found that the measured T_g values are reduced below the bulk value with measured T_g of 341 K for a 6 nm iso-PS. Furthermore, Fakhraai and Forrest[78] recently reported that the T_g depression in thin polystyrene films depends on the cooling rate of the sample; the slower the cooling rate the lower the glass transition temperature. This explains the lack of agreement between the majority of the literature and the recent nano-calorimetry studies performed at much higher cooling rate and measurement frequencies[79]. As suggested by Yasar et al.[80] the glass transition can be measured at different heating rates; each rate would yield different values for T_g. T_g must be accompanied by details of the measuring technique, heating rate, sample molecular weight, and sample pre-treatment.

A summary of glass transition temperatures (T_g) obtained for polystyrene from TMDSC (conventional MDSC and quasi-isothermal MDSC mode), and the literature is shown in Table 4-3. Since the heating rate for polystyrene in this study (2 K/min) is as slow as the heating rate in Fakhraai and Forrest[78] (3 K/min), the glass transition temperature found in this study is consistent with the results reported by Fakhraai and Forrest[78]. Furthermore, it is observed that the measured glass transition temperature for both conventional MDSC and quasi-isothermal MDSC agree within the experimental error (±2 K).

Table 4-3: Summary of the glass transition temperature of polystyrene obtained from the literature, conventional MDSC (3 heating cycles), and quasi-isothermal MDSC

	$T_{glass\ transition}$ (K)
Xu, H. and Cebe, P.[65, 66] (bulk)	377±0.5
Koh, Y. P., McKenna, G. B., Simon, S. L.[79] (bulk)	372.25
Fakhraai, Z., and Forrest, J. A.[78] (6 nm film)	341
Conventional MDSC (Cycle 1) this work	343±2
Conventional MDSC (Cycle 2) this work	343±2
Conventional MDSC (Cycle 3) this work	344±2
Quasi-isothermal MDSC this work	341±2

A comparison between the DSC and TMDSC results for reference materials used in this study and values available in the literature shows that DSC and TMDSC can both detect first order solid-solid transitions, solid-liquid transitions and glass transitions, where the enthalpy of transition is in the order of 1 J/g or greater, but they cannot detect the second

order solid transitions since the energy of this transition is below their detection limits. DSC heat capacity measurements are repeatable to within 0.05 J/(g·K) and are consistent with the literature. Total heat capacity values obtained from TMDSC measurements are not quantitative. Heat capacities obtained from DSC measurements are used instead. Further, reversing heat capacities required calibration with low temperature heat capacities to render them quantitative – conditions where no transitions were occurring. Thus, TMDSC is limited to evaluation of phase transition kinetics. Slow transitions relative to the speed of measurements report as "non-reversing", fast transitions report as "reversing". For example, for the phenanthrene phase transitions, Figure 4-2, most of the sample keeps pace with the temperature fluctuation for the solid-solid transition, while only a small fraction does for the solid-liquid transition. These transitions, as with the glass transition for polystyrene, Figure 4-5, are all reversible in a thermodynamic sense. The reappear when the same sample is subjected to repeated heating cycles.

4.2 – Athabasca Bitumen Asphaltenes Samples

Figure 4-6 (a-c) shows the heat capacities for pentane through dodecane Athabasca Bitumen (AB) asphaltenes obtained from DSC measurements for two successive heating cycles, 4-6 (a) and (b), and the difference between them, Figure 4-6 (c). There is a broad endothermic transition, relative to solid behaviour, beginning at temperatures below 320 K. As asphaltenes are solid at room temperature and liquid at high temperature, this transition reflects a solid or glass to liquid transition. There is also an exothermic transition in the first heating cycle for all Athabasca Bitumen asphaltenes. The apparent heat capacity of liquid or a combination of solid and liquid cannot drop below that of a solid unless there is an exothermic process present. During the second heating cycle, this transition is absent. As the heating cycles were conducted hours apart in time, the exothermic transition is irreversible over this time scale. The transition begins at approximately 380 K and ends at approximately 440 K. The value of the enthalpy of transition is small in all cases and approaches the detection limit for difference measurements. However, the value falls in the 0 to - 4 J/g range.

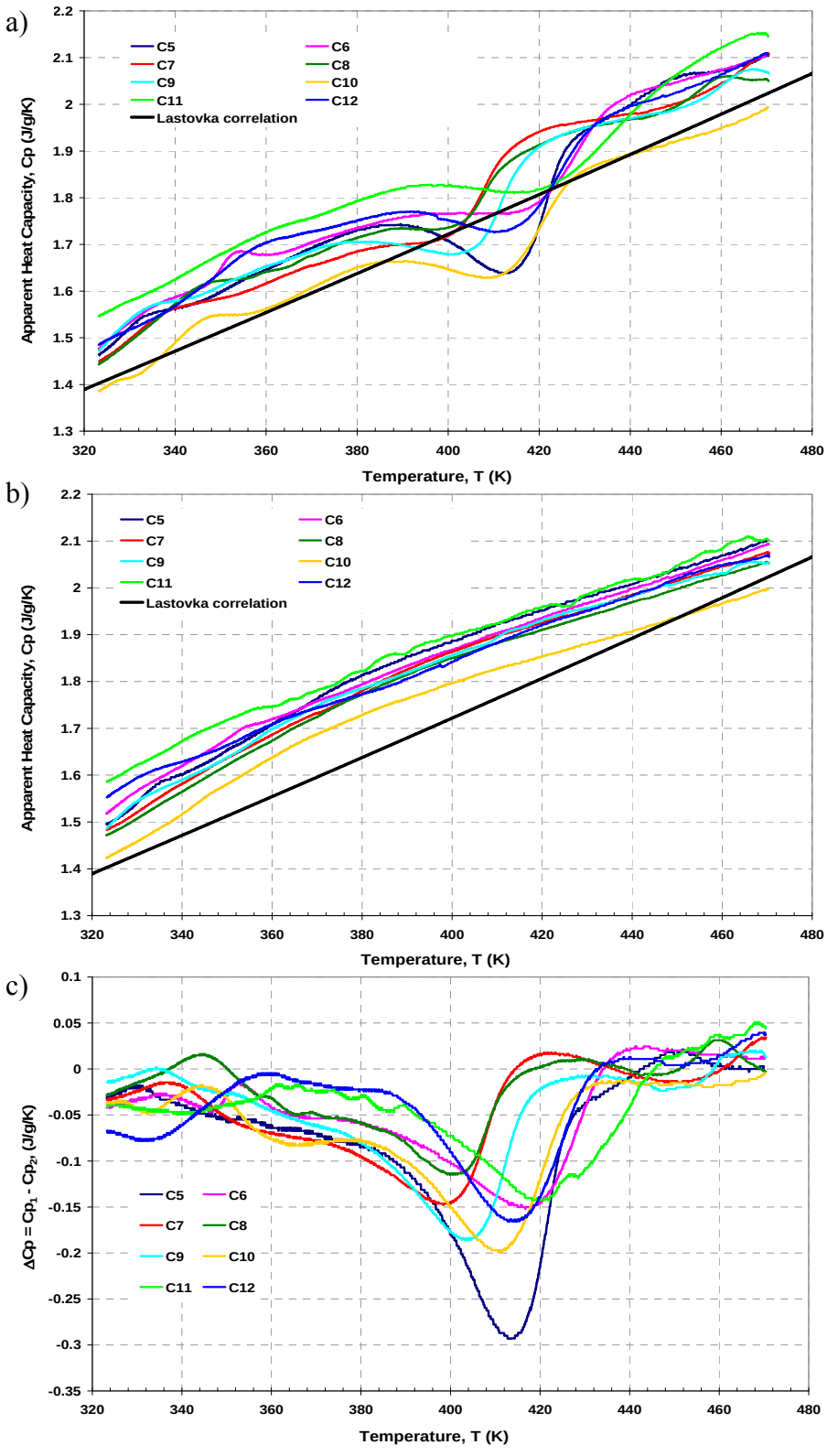

Figure 4-6: Apparent heat capacity obtained from DSC for C_5 through C_{12} Athabasca Bitumen asphaltenes: a) heating cycle 1, b) heating cycle 2, and c) the difference cycle 1- cycle 2

These transitions were explored in greater detail using TMDSC. Figures 4-7 (a) and (b) illustrate the reversing apparent heat capacity for pentane through dodecane Athabasca Bitumen asphaltenes obtained from two successive TMDSC heating cycles. All of the asphaltene samples diverge from the predicted values for solid hydrocarbons at temperatures exceeding 300 K. During the first heating cycle, the apparent heat capacity values differ from one another. For the second heating cycle, they are similar. The difference between the reversing heat capacities, Figure 4-7 (c), falls within the error bounds for difference measurements, ± 0.10 J/(g·K), except for pentane and hexane asphaltenes. This suggests that the thermal behaviour of the pentane and hexane asphaltenes differ from the other asphaltenes.

The magnitude and breadth of the reversible endotherms are illustrated in Figure 4-8 where again the predicted heat capacity for solid hydrocarbons Equation (3.23) is used as a baseline. The upper temperature bounds for transitions to liquid are unclear as the uncertainty of the calorimetric measurement and the values are of the same scale but a value exceeding 450 K is indicated. Again, the enthalpy of the transition is small and uncertain because the difference between the apparent heat capacity of the samples and the heat capacity of a solid approaches the detection limits and the transition is broad. A value in the order of 10 J/g is a reasonable estimate. The upper bound temperature is consistent with reported values by Gray et al.[36] for Athabasca asphaltenes, 478 K – 507 K with a standard deviation of 16 K, and Zhang et al.[35] who reported melting temperatures for four other asphaltenes 493 K – 513 K. These latest results differ from prior work in that the lower bound of the phase transition is also identified. Thus, the asphaltenes comprise a minimum of two phases, one solid like and one liquid like, over a broad temperature range. Given the magnitude of the enthalpy of transition, the low temperature phase is likely to be a glass. Enthalpies of fusion, for organic solids are one order of magnitude higher, as shown in Figures 4-1 and 4-2 for hexadecane and phenanthrene.

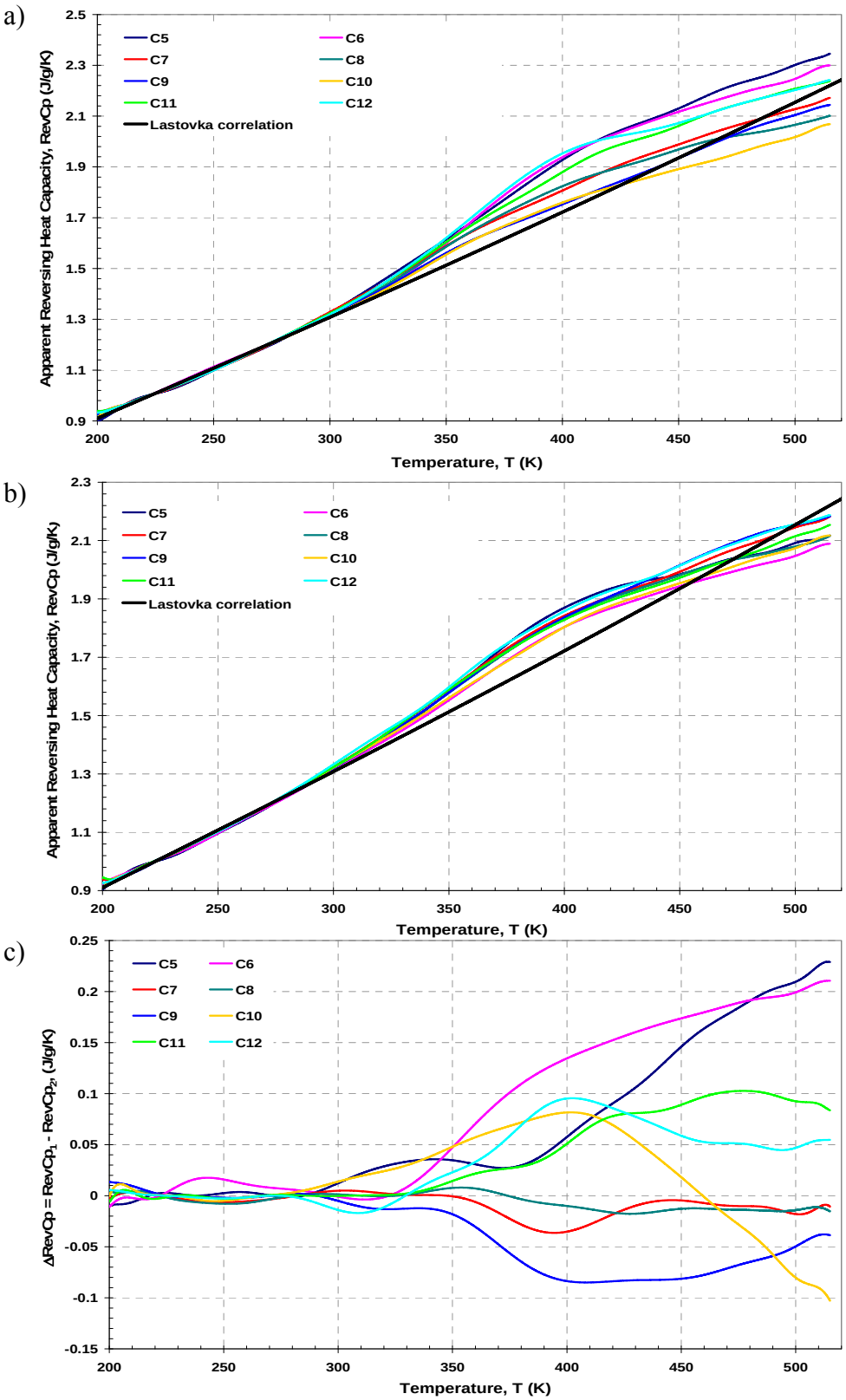

Figure 4-7: Reversing heat capacity for C_5 through C_{12} Athabasca Bitumen asphaltenes obtained from TMDSC: a) heating cycle 1, b) heating cycle 2, and c) cycle 1– cycle 2.

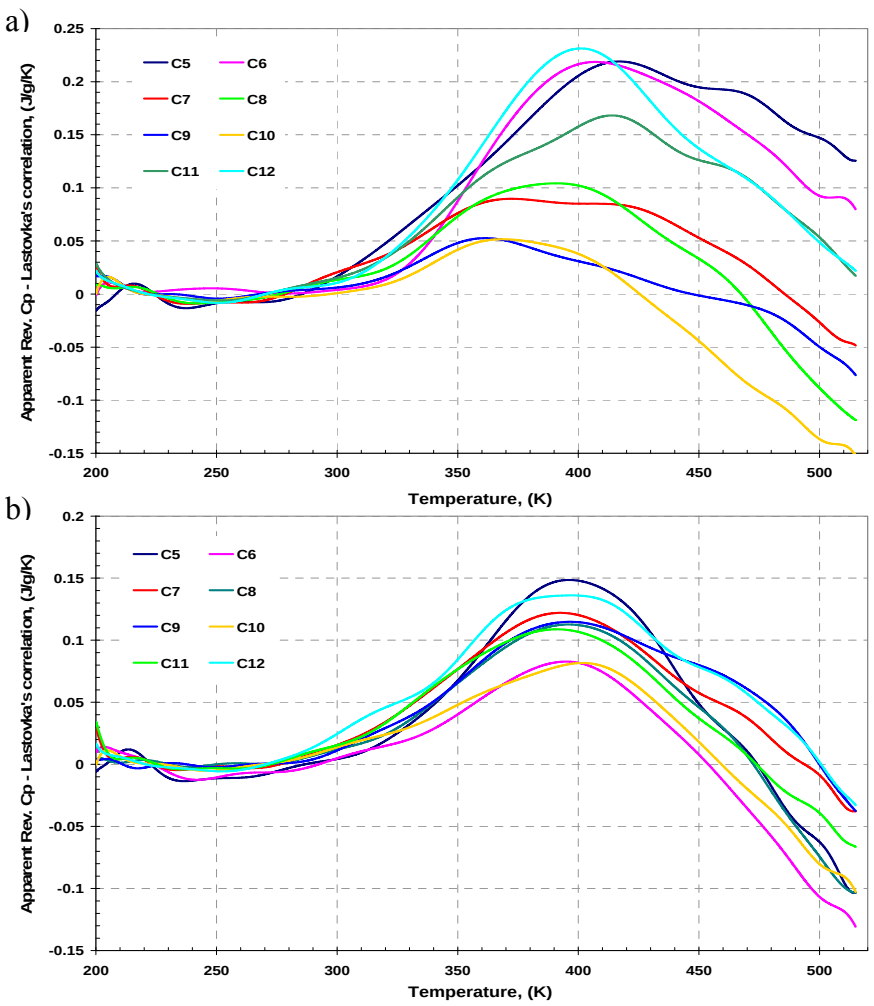

Figure 4-8: Difference between reversing heat capacity and Lastovka's correlation for C_5 through C_{12} Athabasca bitumen asphaltenes, a) heating cycle 1 and b) heating cycle 2

Non-reversing heat capacities for Athabasca asphaltenes were obtained from the difference between the total heat capacity, obtained from DSC measurements, and the reversing heat capacity obtained from TMDSC measurements, normalized with respect to low temperature solid heat capacities, Equation (3.23), where the reversing and total heat capacities coincide. The non-reversing heat capacities for the first and second heating cycles are reported in Figures 4-9 (a) & (b). As the exotherm is absent from the second heating cycle, the difference between first and second heating cycle non-reversing heat capacities, for C_5 through C_{12} Athabasca asphaltenes are reported in Figure 4-9 (c). The irreversible transition is thus parsed from other kinetically slow but reversible transitions. As expected, Figure 4-9 (c) and Figure 4-6 (c) are in agreement.

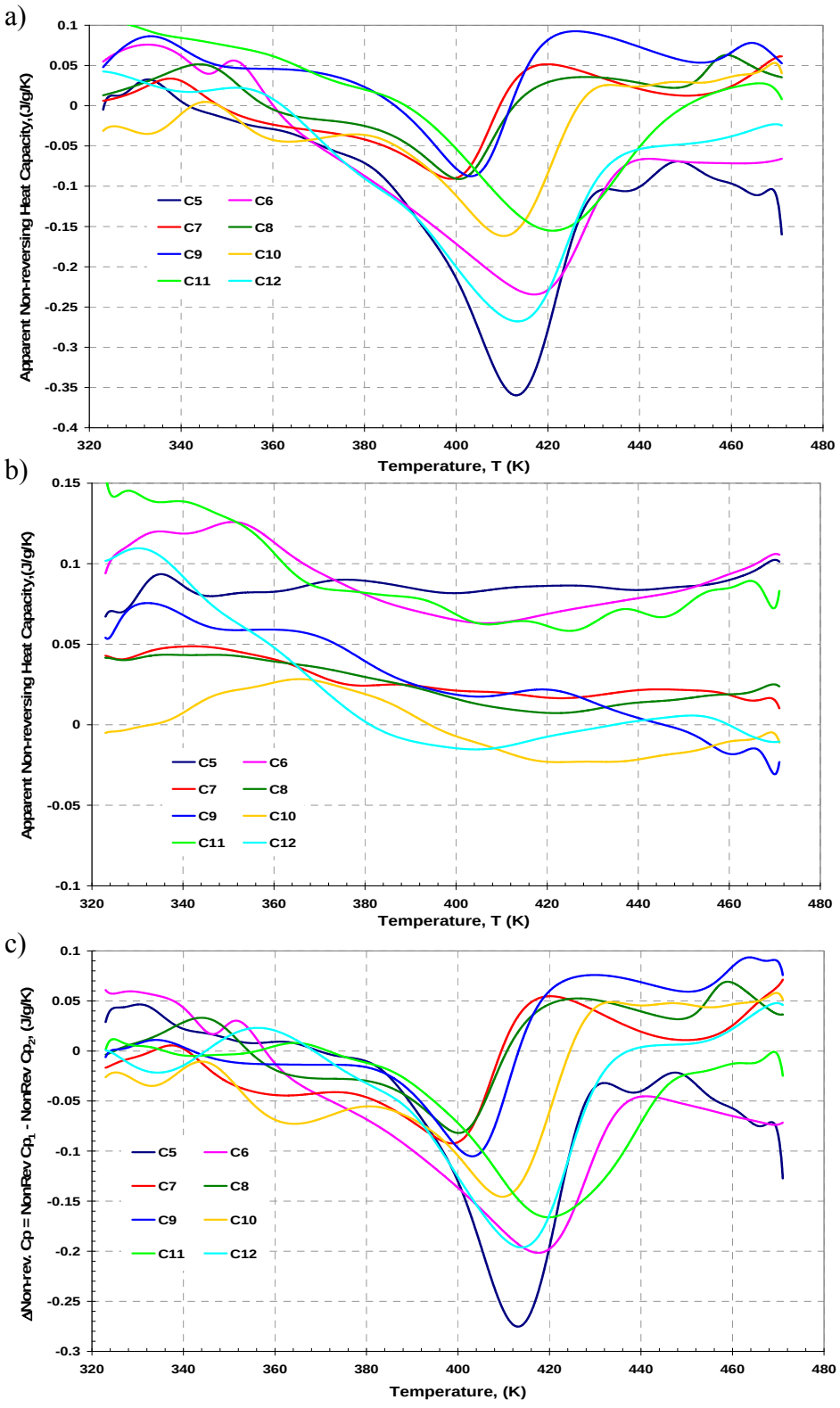

Figure 4-9: Non-reversing heat capacity for C_5 through C_{12} Athabasca bitumen asphaltenes obtained from TMDSC: a) heating cycle 1, b) heating cycle 2, and c) cycle 1– cycle 2.

The reproducibility of reversing and non-reversing measurements was tested with C_6, C_7, C_8, and C_{10} Athabasca asphaltenes. Figures 4-11 and 4-12 illustrate the reproducibility for reversing and non-reversing heat capacities, respectively. Repeated measurements, with different samples for C_6, C_7, C_8, and C_{10} Athabasca asphaltenes show the same trends for start and end temperatures and enthalpies of transition for both the endothermic and exothermic transitions.

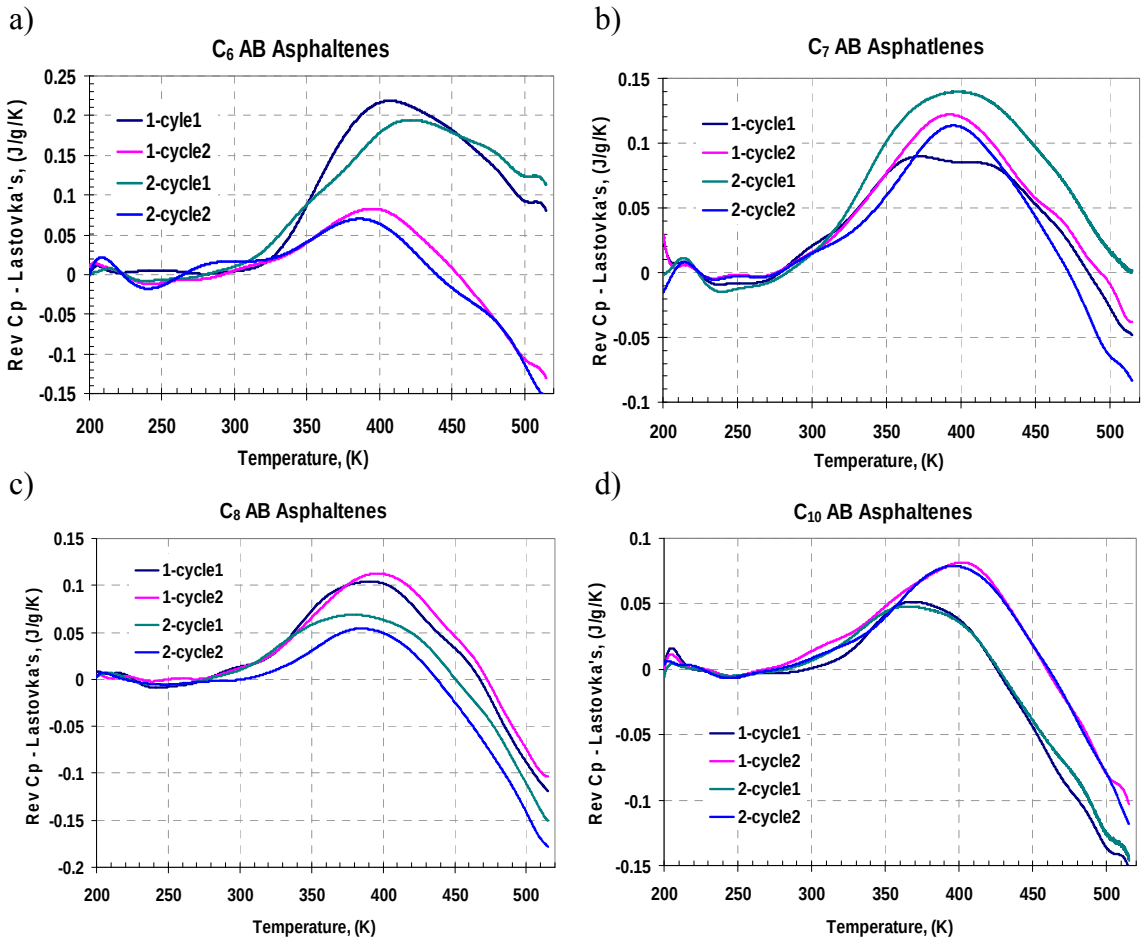

Figure 4-10: Reproducibility of reversing heat capacity for C_6, C_7, C_8, and C_{10} Athabasca Bitumen asphaltenes; the first number is sample number, and the second number is heating cycle number

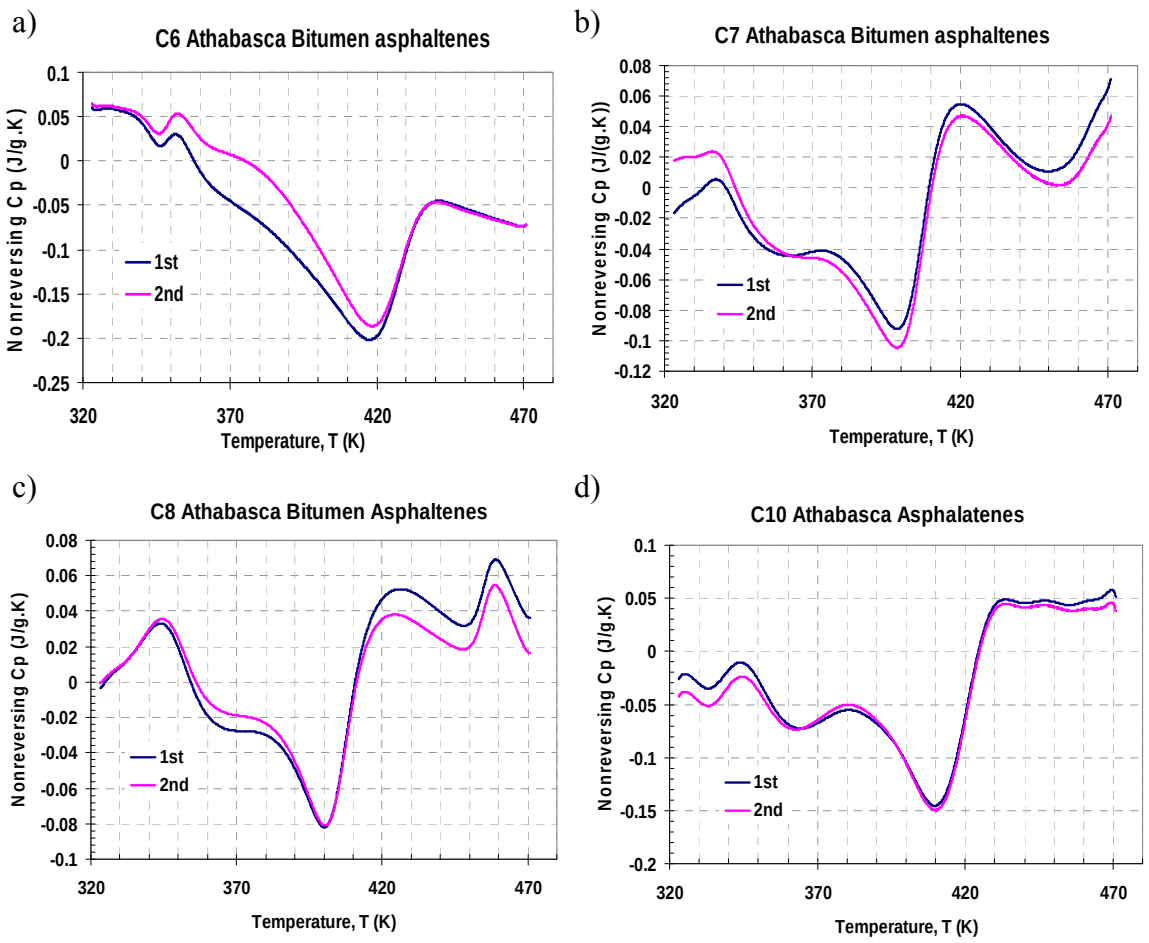

Figure 4-11: Reproducibility on non-reversing heat capacity for C_6, C_7, C_8, and C_{10} Athabasca Bitumen asphaltenes

The start and end temperatures for the exothermic transitions for Athabasca asphaltene samples, including reproduced measurements, are presented in Table 4-4 and plotted in Figure 4-12. The values have a measurement error of ± 5 K. All of the Athabasca asphaltenes start their exothermic transitions at 383 ± 5 K but the end temperatures of the exothermic transitions differ systematically with asphaltene type. For C_7 through C_{12} Athabasca asphaltenes, the end temperature increases with *n*-alkane number. The upper bounds for the exothermic transitions for C_5 and C_6 Athabasca asphaltenes are similar to one another but do not follow the trend of the other asphaltene types. The difference between the behaviour of C_6 and C_7 asphaltenes is striking. Clearly pentane and hexane asphaltenes possess qualitatively different irreversible phase behaviours from the other asphaltenes.

Table 4-4: Start and end temperatures for non-reversing heat capacity for C_5 through C_{12} Athabasca bitumen asphaltenes

	C_5	C_6	C_7	C_8	C_9	C_{10}	C_{11}	C_{12}
Start temperature, T_1 (K)	392	378	379	382	384	386	388	377
End temperature, T_2 (K)	428	435	413	414	417	428	447	432
Start temperature, T_1 (K)		384	376	381		386		
End temperature, T_2 (K)		435	414	415		428		

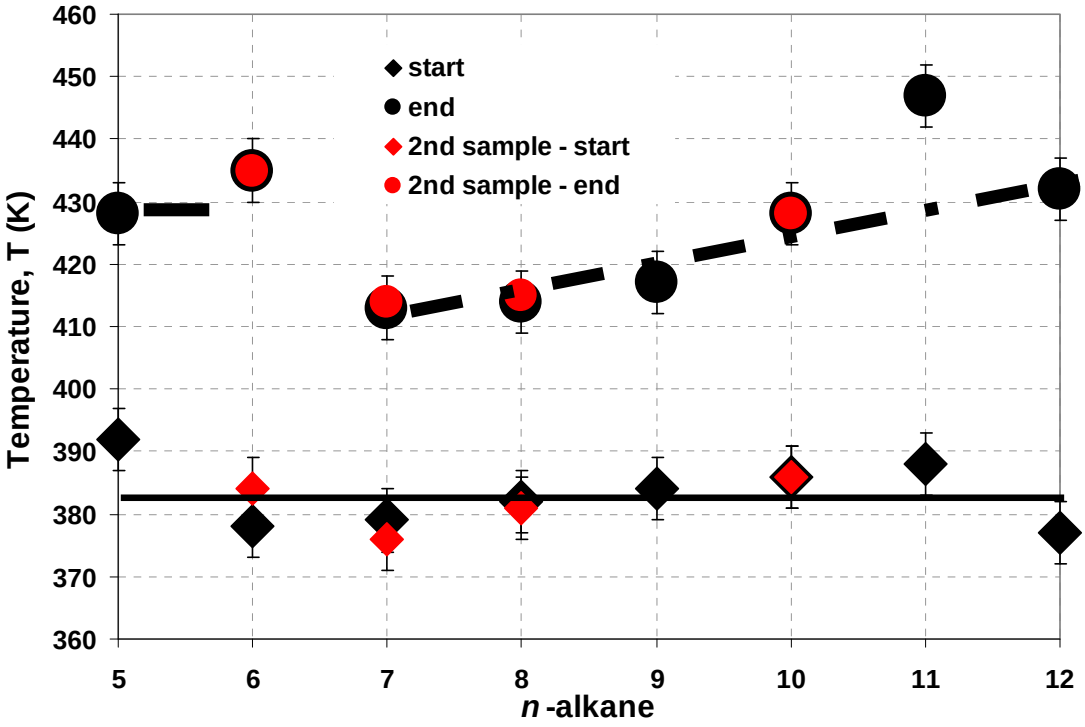

Figure 4-12: Start and end temperatures for the irreversible transition occurring in C_5 - C_{12} Athabasca asphaltenes obtained from the non-reversing apparent heat capacity.

Ancillary Measurements

While samples are hermitically sealed during calorimetric measurements, there is always concern that differences arising in successive heating cycles might arise from mass loss during the performance of experiments. Repeated thermogravimetric analysis performed approximately 10 mg of pentane Athabasca bitumen asphaltenes shows that there is only ppmw level volatilization between 320 K and 400 K and on average 1.3 wt % volatilizes

at 570 K, *in an open vessel* - Figure 4-14. Zhang et al.[35] reported a 0.5 wt % loss at 573 K for a heptane Iranian Light asphaltene sample. Zhang et al.[35] attributed mass loss to the possible evaporation of low-molecular-weight components and the release of adsorbed gases. These are clearly not significant effects in the calorimetric measurements performed here.

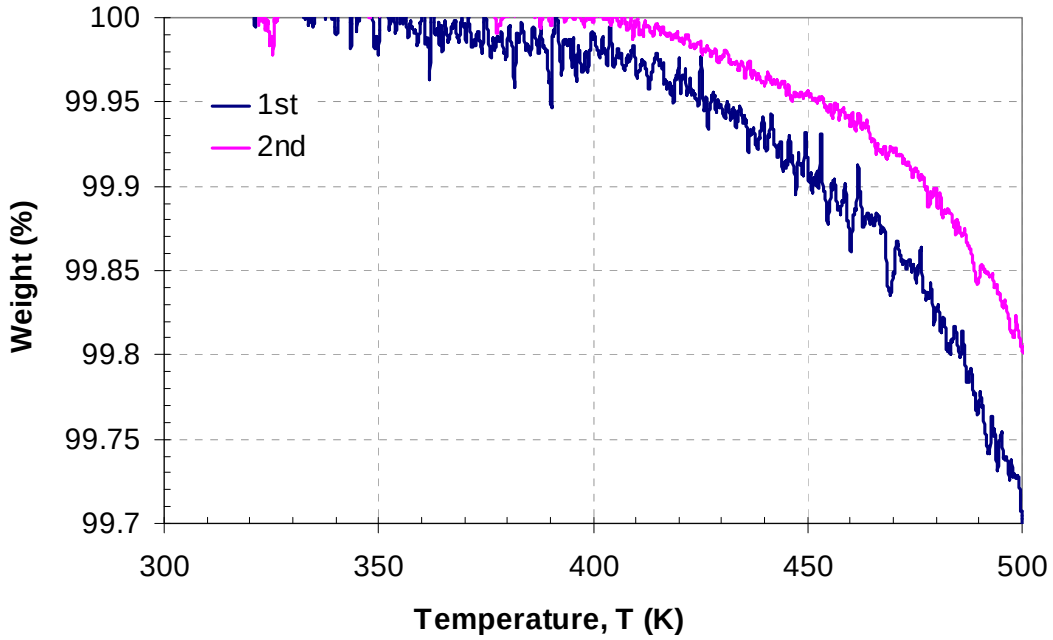

Figure 4-13: TGA results for 2 pentane Athabasca asphaltene samples from room temperature to 500 K with the heating rate of 10 K/min

Interpretation

Fulem at al.[29] reported a broad endothermic transition from an amorphous solid to liquid over the temperature interval 340 K to 520 K for Maya pentane asphaltenes using a combination of DSC and phase angle measurements. They also observed an overlapping exotherm during the endothermic transition for Maya pentane asphaltenes, on first heating. Fulem at al.[29] suggested that the presence of the overlapping exotherm was consistent with a fraction of solid asphaltenes dissolving into liquid asphaltenes. The results reported here for Athabasca bitumen pentane through dodecane asphaltenes, provide direct evidence for the two overlapping transitions, and are qualitatively

consistent with this prior work. The behaviour they observed appears to be a general one as it is insensitive to asphaltene source and asphaltene definition.

CHAPTER 5 - CONCLUSIONS and FUTURE WORK

5.1 – Conclusions

Experiments performed with reference samples highlighted the contrasting advantages for DSC (heat capacity) and TMDSC (phase transition enthalpy and kinetics) and identified their respective limitations related to investigation of phase transitions with small enthalpies of transition spread over broad temperature ranges. Asphaltene phase transition measurement approaches the limits of detect-ability. The temperature and heat capacity errors are within 5%.

For Athabasca bitumen pentane through dodecane asphaltenes, two phase transitions have been identified over the temperature interval 200 K to 525 K using a combination of DSC and TMDSC measurements.

Athabasca bitumen asphaltenes exhibit a broad and reversible endothermic transition from solid or glass to liquid starting at ~ 300 K and extending over most of the balance of the temperature interval. The endothermic transition is qualitatively similar for all of the asphaltenes.

Asphaltenes exhibit a minimum of two phases over the temperature interval 300 K to more than 500 K.

There is a second transition starting at 383 ± 5 K and ending in the mid 400 K range. This transition is exothermic and is irreversible on the time scale of hours.

The enthalpies of transition for both the endothermic and exothermic transitions are small. The endotherm possesses an enthalpy of the order of 10 J/g while the enthalpy for the exotherm is less than 4 J/g.

The exotherms for pentane and hexane asphaltenes are qualitatively different from the exotherms for heptane through dodecane asphaltenes. Trends in end temperatures for the exotherms for these two asphaltene groups differ significantly.

Details of the phase behaviour and thermophysical properties of the Athabasca bitumen asphaltenes are joint functions of their definition and their thermal history. For example, the phase behaviour and thermophysical properties of individual asphaltenes, e.g. Athabasca bitumen pentane asphaltenes, at ambient conditions, are expected to differ depending on their thermal history above 380 K. The properties of pentane asphaltenes differ from heptane asphaltenes subjected to the same thermal history in the 380 K to 420 K temperature range.

5.2 – Future work

Perform sample reheating experiments following long soak periods at ambient temperature to assess whether the irreversible transition identified in this study is merely slowly reversible.

Repeat this study with asphaltenes drawn from one or more other feed stocks such as Maya crude oil.

Study the fraction of asphaltenes undergoes the exothermic transition.

REFERENCES

1. Trejo, F.; Centeno, G.; Ancheyta, J., Precipitation, fractionation and characterization of asphaltenes from heavy and light crude oils. *Fuel* **2004,** 83, (16), 2169-2175.
2. Calemma, V.; Iwanski, P.; Nali, M.; Scotti, R.; Montanari, L., Structural characterization of asphaltenes of different origins. *Energy & Fuels* **1995,** 9, (2), 225-230.
3. Alboudwarej, H.; Akbarzadeh, K.; Beck, J.; Svrcek, W. Y.; Yarranton, H. W., Regular solution model for asphaltene precipitation from bitumens and solvents. *AIChE Journal* **2003,** 49, (11), 2948-2956.
4. Speight, J. G., *The chemistry and technology of petroleum*. New York: Marcel Dekker: 1999.
5. Calemma, V.; Rausa, R.; D'Antona, P.; Montanari, L., Characterization of asphaltenes molecular structure. *Energy & Fuels* **1998,** 12, (2), 422-428.
6. Sheremata, J. M.; Gray, M. R.; Dettman, H. D.; McCaffrey, W. C., Quantitative molecular representation and sequential optimization of Athabasca asphaltenes. *Energy and Fuels* **2004,** 18, (5), 1377-1384.
7. Pacheco-Sanchez, J. H.; Mansoori, G. A., Prediction of the phase behavior of asphaltene micelle aromatic hydrocarbon systems. *Petroleum Science and Technology* **1998,** 16, (3-4), 377-394.
8. Takanohashi, T.; Sato, S.; Tanaka, R., Structural relaxation behaviors of three different asphaltenes using MD calculations. *Petroleum Science and Technology* **2004,** 22, (7-8), 901-914.
9. Leon, O.; Rogel, E.; Espidel, J.; Torres, G., Asphaltenes: Structural characterization, self-association, and stability behavior. *Energy and Fuels* **2000,** 14, (1), 6-10.
10. Hutton, A. C., Petrographic classification of oil shales. *International Journal of Coal Geology* **1987,** 8, (3), 203-231.
11. Lastovka, V.; Fulem, M.; Becerra, M.; Shaw, J. M., A similarity variable for estimating the heat capacity of solid organic compounds Part II - application: heat

capacity calculation for ill-defined organic solids. *Fluid Phase Equilibria* In Press, Accepted Manuscript.

12. Lastovka, V.; Shaw, J. M., Predictive correlation for Cp of organic solids based on elemental composition. *Journal of Chemical and Engineering Data* **2007,** 52, (4), 1160-1164.
13. Zhao, B.; Shaw, J. M., Composition and size distribution of coherent nanostructures in Athabasca bitumen and Maya crude oil. *Energy & Fuels* **2007,** 21, (5), 2795-2804.
14. Zhao, B.; Zhang, X. H.; Shaw, J. M., Interplay between the physical properties of Athabasca bitumen plus diluent mixtures and coke deposition on a commercial hydroprocessing catalyst. *Energy & Fuels* **2008,** 22, (3), 1747-1758.
15. Meyers, P. A., Composition and properties of petroleum (Book). *American Scientist* **1982,** 70, (4), 416.
16. Speight, J. G., Thermal transformations of asphaltenes. *Petroleum Chemistry U.S.S.R.* **1989,** 29, (4), 253-261.
17. Speight, J. G.; Long, R. B.; Trowbridge, T. D., Factors influencing the separation of asphaltenes from heavy petroleum feedstocks. *Fuel* **1984,** 63, (5), 616-620.
18. Yarranton, H. W.; Masliyah, J. H., Molar mass distribution and solubility modeling of asphaltenes. *Aiche Journal* **1996,** 42, (12), 3533-3543.
19. Wiehe, I. A.; Liang, K. S., Asphaltenes, resins, and other petroleum macromolecules. *Fluid Phase Equilibria* **1996,** 117, (1-2), 201-210.
20. Mitchell, D. L.; Speight, J. G., The solubility of asphaltenes in hydrocarbon solvents. *Fuel* **1973,** 52, (2), 149-152.
21. Redelius, P. G., Solubility parameters and bitumen. *Fuel* **2000,** 79, (1), 27-35.
22. Schabron, J. F.; Pauli, A. T.; Rovani, J. F., Molecular weight polarity map for residua pyrolysis. *Fuel* **2001,** 80, (4), 529-537.
23. Wiehe, I. A., Two-dimensional solubility parameter mapping of heavy oils. *Fuel Science & Technology International* **1996,** 14, (1-2), 289-312.
24. Orangi, H. S.; Modarress, H.; Fazlali, A.; Namazi, M. H., Phase behavior of binary mixture of asphaltene plus solvent and ternary mixture of asphaltene plus solvent plus precipitant. *Fluid Phase Equilibria* **2006,** 245, (2), 117-124.

25. Sirota, E. B.; Lin, M. Y., Physical behavior of asphaltenes. *Energy & Fuels* **2007,** 21, 2809-2815.
26. Evdokimov, I. N.; Eliseev, N. Y.; Akhmetov, B. R., Initial stages of asphaltene aggregation in dilute crude oil solutions: studies of viscosity and NMR relaxation. *Fuel* **2003,** 82, (7), 817-823.
27. Evdokimov, I. N.; Eliseev, N. Y.; Akhmetov, B. R., Assembly of asphaltene molecular aggregates as studied by near-UV/visible spectroscopy - II. Concentration dependencies of absorptivities. *Journal of Petroleum Science and Engineering* **2003,** 37, (3-4), 145-152.
28. Sirota, E. B., Physical structure of asphaltenes. *Energy & Fuels* **2005,** 19, (4), 1290-1296.
29. Fulem, M.; Becerra, M.; Hasan, A.; Zhao, B.; Shaw, J. M., Phase behaviour of Maya crude oil based on calorimetry and rheometry. *Fluid Phase Equilibria* In Press, Accepted Manuscript.
30. Dickie, J. P.; Yen, T. F., Macrostructures of Asphaltic Fractions by Various Instrumental Methods. *Analytical Chemistry* **1967,** 39, (14), 1847-&.
31. Barbour, R. V.; Petersen, J. C., Molecular-Interactions of Asphalt - Infrared Study of Hydrogen-Bonding Basicity of Asphalt. *Analytical Chemistry* **1974,** 46, (2), 273-277.
32. Moschopedis, S. E.; Speight, J. G., Investigation of Hydrogen-Bonding by Oxygen Functions in Athabasca Bitumen. *Fuel* **1976,** 55, (3), 187-192.
33. Joshi, N. B.; Mullins, O. C.; Jamaluddin, A.; Creek, J.; McFadden, J., Asphaltene precipitation from live crude oil. *Energy & Fuels* **2001,** 15, (4), 979-986.
34. Buenrostro-Gonzalez, E.; Lira-Galeana, C.; Gil-Villegas, A.; Wu, J. Z., Asphaltene precipitation in crude oils: Theory and experiments. *Aiche Journal* **2004,** 50, (10), 2552-2570.
35. Zhang, Y.; Takanohashi, T.; Sato, S.; Saito, I.; Tanaka, R., Observation of glass transition in asphaltenes. *Energy & Fuels* **2004,** 18, (1), 283-284.
36. Gray, M. R.; Assenheimer, G.; Boddez, L.; McCaffrey, W. C., Melting and fluid behavior of asphaltene films at 200-500 degrees C. *Energy & Fuels* **2004,** 18, (5), 1419-1423.

37. Maham, Y.; Chodakowski, M. G.; Zhang, X.; Shaw, J. M., Asphaltene phase behavior: prediction at a crossroads. *Fluid Phase Equilibria* **2005,** 227, (2), 177-182.

38. Hohne, G. W. H., Hemminger, W. F., Flammersheim, H.-J., *Differential scanning calorimetry*. 2nd rev. ed.; Springer - Verlag Berlin Heidelberg New York: 2003; p 298.

39. Höhne, G. W. H., Problems with the calibration of differential-temperature-scanning-calorimeters. *Thermochimica Acta* **1983,** 69, (1-2), 175-197.

40. Marini, A.; Berbenni, V.; Flor, G.; Massarotti, V.; Riccardi, R., An analysis of the factors affecting the peak shape and the quantitative reliability of a heat flux DSC cell. *Thermochimica Acta* **1985,** 95, (2), 419-424.

41. Farkas, J.; MohacsiFarkas, C., Application of differential scanning calorimetry in food research and food quality assurance. *Journal of Thermal Analysis* **1996,** 47, (6), 1787-1803.

42. Taylor, M. K.; Hickey, A. J.; VanOort, M., Manufacture, characterization, and pharmacodynamic evaluation of engineered ipratropium bromide particles. *Pharmaceutical Development and Technology* **2006,** 11, (3), 321-336.

43. Wu, J. J.; Reading, M.; Craig, D. Q. A., Application of calorimetry, sub-ambient atomic force microscopy and dynamic mechanical analysis to the study of frozen aqueous trehalose solutions. *Pharmaceutical Research* **2008,** 25, (6), 1396-1404.

44. Sadeghi, F.; Tremblay, A. Y.; Kruczek, B., Synthesis and characterization of emulsion polymerized mixed matrix aluminum silicate/poly(2,6-dimethyl 1,4-phenylene oxide) films. *Journal of Applied Polymer Science* **2008,** 109, (3), 1454-1460.

45. Wu, X. B.; Chen, J. Q.; Zeng, Z. R., The Application of Dsc in Identification of Ldpe/Lldpe Blends Mulching Film. *Angewandte Makromolekulare Chemie* **1991,** 189, 183-193.

46. Corbino, O. M., Thermal oscillations in lamps of thin fibers with alternating current flowing through them and the resulting effect on the rectifier as a result of the presence of even-numbered harmonics. *Physikalische Zeitschrift* **1910,** 11, 413-417.

47. Corbino, O. M., Periodic resistance changes of fine metal threads, which are brought together by alternating streams as well as deduction of their thermo characteristics at high temperatures. *Physikalische Zeitschrift* **1911,** 12, 292-295.

48. Gobrecht, H.; Hamann, K.; Willers, G., Complex plane analysis of heat capacity of polymers in glass transition region. *Journal of Physics E-Scientific Instruments* **1971,** 4, (1), 21-&.

49. Jiang, Z.; Imrie, C. T.; Hutchinson, J. M., An introduction to temperature modulated differential scanning calorimetry (TMDSC): a relatively non-mathematical approach. *Thermochimica Acta* **2002,** 387, (1), 75-93.

50. Reading, M.; Elliott, D.; Hill, V. L., A new approach to the calorimetric investigation of physical and chemical-transitions. *Journal of Thermal Analysis* **1993,** 40, (3), 949-955.

51. Reading, M.; Luget, A.; Wilson, R., Modulated differential scanning calorimetry. *Thermochimica Acta* **1994,** 238, 295-307.

52. Lacey, A. A.; Nikolopoulos, C.; Reading, M., A mathematical model for modulated differential scanning calorimetry. *Journal of Thermal Analysis* **1997,** 50, (1-2), 279-333.

53. Reading, M., A personal perspective on the rise of MTDSC. *Journal of Thermal Analysis and Calorimetry* **1998,** 54, (2), 411-418.

54. Reading, M.; Luyt, R., MTDSC at the glass transition - Quantitative use of the phase lag correction - The effects of long annealing times. *Journal of Thermal Analysis and Calorimetry* **1998,** 54, (2), 535-544.

55. Schawe, J. E. K., Principles for the interpretation of modulated temperature DSC measurements .1. Glass-transition. *Thermochimica Acta* **1995,** 261, 183-194.

56. Simon, S. L., Temperature-modulated differential scanning calorimetry: theory and application. *Thermochimica Acta* **2001,** 374, (1), 55-71.

57. Wunderlich, B., Glass transition as a key to identifying solid phases. *Journal of Applied Polymer Science* **2007,** 105, (1), 49-59.

58. Wunderlich, B., The glass transition of polymer crystals. *Thermochimica Acta* **2006,** 446, (1-2), 128-134.

59. Wunderlich, B.; Okazaki, I.; Ishikiriyama, K.; Boller, A., Melting by temperature-modulated calorimetry. *Thermochimica Acta* **1998,** 324, (1-2), 77-85.

60. Boller, A.; Schick, C.; Wunderlich, B., Modulated differential scanning calorimetry in the glass transition region. *Thermochimica Acta* **1995,** 266, 97-111.

61. Chen, W.; Moon, I. K.; Wunderlich, B., Study of crystallization kinetics by temperature-modulated DSC. *Polymer* **2000,** 41, (11), 4119-4125.

62. Luyt, A. S.; Vosloo, H. C. M.; Reading, M., Thermoanalytical characterization of polyphenylacetylene - III. Use of modulated differential scanning calorimetry (MDSC). *Thermochimica Acta* **1998,** 320, (1-2), 135-140.

63. Takegawa, K.; Fukao, K.; Saruyama, Y., Aging effects on the thermal expansion coefficient and the heat capacity of glassy polystyrene studied with simultaneous measurement using temperature modulation technique. *Thermochimica Acta* **2007,** 461, (1-2), 67-71.

64. Xu, H.; Cebe, P., Evaluation of the reversible contribution to the reversing heat capacity in isotactic polystyrene. *Thermochimica Acta* **2006,** 442, (1-2), 42-47.

65. Xu, H.; Cebe, P., Heat capacity study of solution grown crystals of isotactic polystyrene. *Macromolecules* **2005,** 38, (3), 770-779.

66. Xu, H.; Cebe, P., Heat capacity study of isotactic polystyrene: Dual reversible crystal melting and relaxation of rigid amorphous fraction. *Macromolecules* **2004,** 37, (8), 2797-2806.

67. Masson, J. F.; Polomark, G. M., Bitumen microstructure by modulated differential scanning calorimetry. *Thermochimica Acta* **2001,** 374, (2), 105-114.

68. Masson, J. F.; Polomark, G. M., Bitumen microstructure by modulated differential scanning calorimetry (vol 374, pg 105, 2001). *Thermochimica Acta* **2004,** 413, (1-2), 273-273.

69. Masson, J. F.; Polomark, G. M.; Collins, P., Time-dependent microstructure of bitumen and its fractions by modulated differential scanning calorimetry. *Energy & Fuels* **2002,** 16, (2), 470-476.

70. Marti, E.; Kaisersberger, E.; Moukhina, E., Heat capacity functions of polystyrene in glassy and in liquid amorphous state and glass transition DSC and TMDSC study. *Journal of Thermal Analysis and Calorimetry* **2006,** 85, (2), 505-525.

71. Cammenga, H. K.; Eysel, W.; Gmelin, E.; Hemminger, W.; Höhne, G. W. H.; Sarge, S. M., The temperature calibration of scanning calorimeters : Part 2. Calibration substances. *Thermochimica Acta* **1993,** 219, 333-342.

72. Höhne, G. W. H.; Cammenga, H. K.; Eysel, W.; Gmelin, E.; Hemminger, W., The temperature calibration of scanning calorimeters. *Thermochimica Acta* **1990,** 160, (1), 1-12.

73. Sarge, S. M.; Gmelin, E.; Höhne, G. W. H.; Cammenga, H. K.; Hemminger, W.; Eysel, W., The caloric calibration of scanning calorimeters. *Thermochimica Acta* **1994,** 247, (2), 129-168.

74. Sarge, S. M.; Hemminger, W.; Gmelin, E.; Hohne, G. W. H.; Cammenga, H. K.; Eysel, W., Metrologically based procedures for the temperature, heat and heat flow rate calibration of DSC. *Journal of Thermal Analysis* **1997,** 49, (2), 1125-1134.

75. Sabbah, R.; Xu-wu, A.; Chickos, J. S.; Leitão, M. L. P.; Roux, M. V.; Torres, L. A., Reference materials for calorimetry and differential thermal analysis. *Thermochimica Acta* **1999,** 331, (2), 93-204.

76. Chirico, R. D.; Knipmeyer, S. E.; Steele, W. V., Heat capacities, enthalpy increments, and derived thermodynamic functions for naphthalene between the temperatures 5 K and 440 K. *The Journal of Chemical Thermodynamics* **2002,** 34, (11), 1873-1884.

77. Finke, H. L.; Messerly, J. F.; Lee, S. H.; Osborn, A. G.; Douslin, D. R., Comprehensive thermodynamic studies of seven aromatic hydrocarbons. *The Journal of Chemical Thermodynamics* **1977,** 9, (10), 937-956.

78. Fakhraai, Z.; Forrest, J. A., Probing slow dynamics in supported thin polymer films. *Physical Review Letters* **2005,** 95, (2).

79. Koh, Y. P.; McKenna, G. B.; Simon, S. L., Calorimetric glass transition temperature and absolute heat capacity of polystyrene ultrathin films. *Journal of Polymer Science Part B-Polymer Physics* **2006,** 44, (24), 3518-3527.

80. Yasar, M.; Akmaz, S.; Gurkaynak, M. A., Investigation of glass transition temperatures of Turkish asphaltenes. *Fuel* **2007,** 86, (12-13), 1737-1748.

APPENDIX A:

TMDSC Data for Phenanthrene with fixed heating rate, different amplitude and frequency

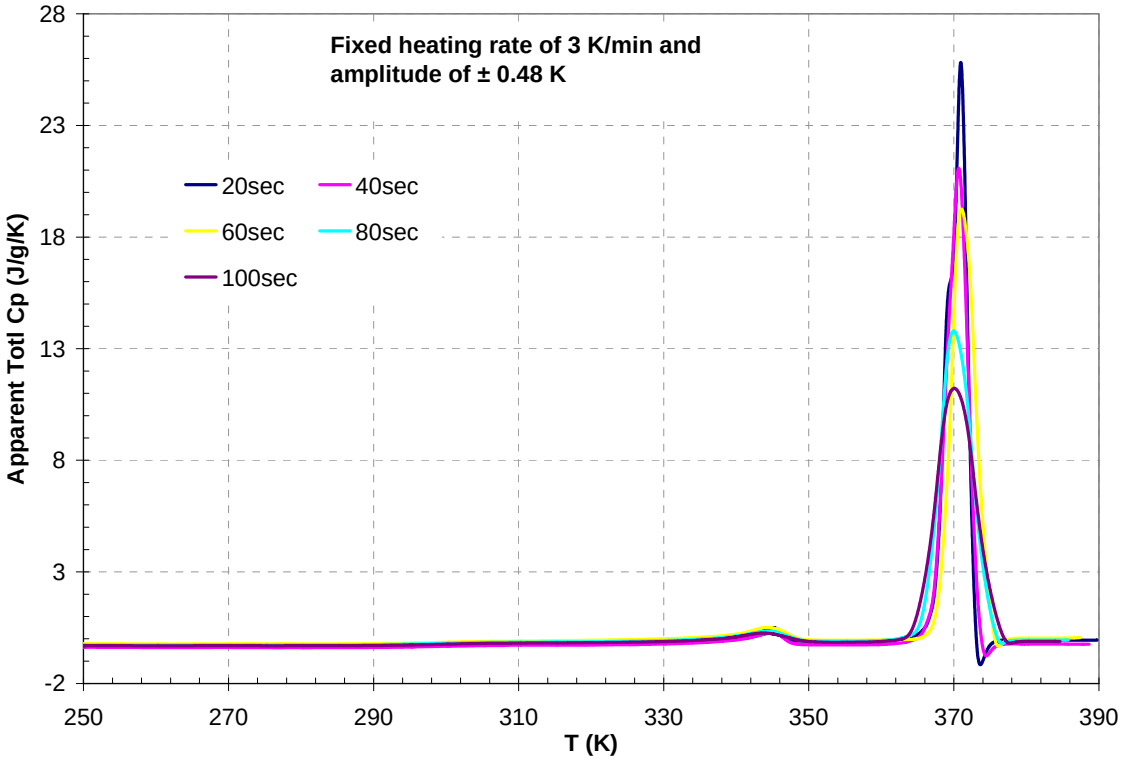
Fixed heating rate of 3 K/min and
amplitude of ± 0.48 K
20sec
40sec
60sec
80sec
100sec
Apparent Totl Cp (J/g/K)
28
23
18
13
8
3
-2
250
270
290
310
330
350
370
390
T (K)

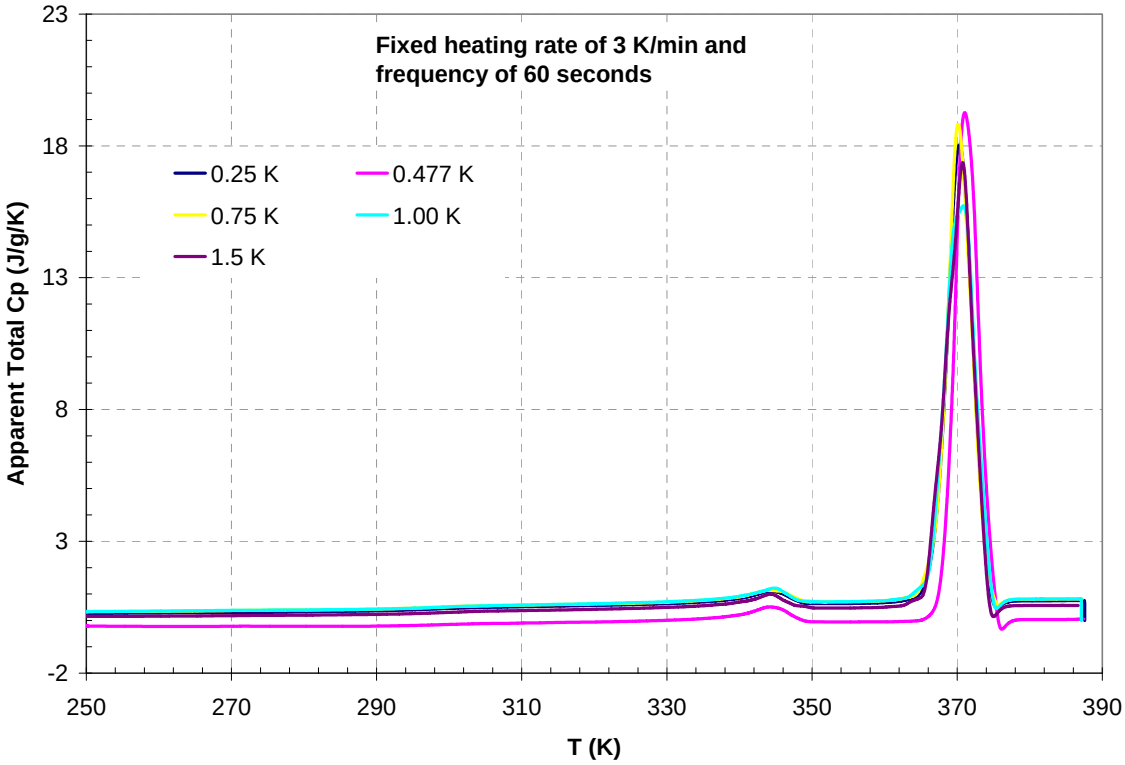
Fixed heating rate of 3 K/min and
frequency of 60 seconds
0.25 K
0.477 K
0.75 K
1.00 K
1.5 K
Apparent Total Cp (J/g/K)
23
18
13
8
3
-2
250
270
290
310
330
350
370
390
T (K)